

Search and characterization of third bodies around binary systems using data from Kepler and TESS satellites

2 JEFFERSON R. P. INÁCIO,¹ ISAAC M. MACÊDO,¹ ÉDER V. X. FERREIRA,² RONAI LISBOA,² TARCIRO N. C. MENDES,²
3 MARILDO G. PEREIRA,³ JOSÉ R. P. DA SILVA,¹ AND LEONARDO A. ALMEIDA^{2,1}

4 ¹*Universidade do Estado do Rio Grande do Norte, Mossoró, RN, Brazil*

5 ²*Universidade Federal do Rio Grande do Norte, Natal, RN, Brazil*

6 ³*Universidade Estadual de Feira de Santana, Feira de Santana, BA, Brazil*

ABSTRACT

The study of the orbital period variation of short-period binary systems has been important to understand several physical phenomena, such as the emission of gravitational waves, angular momentum loss via magnetic braking, matter transfer between the components, apsidal motion, quadrupole moment variation and presence of circumbinary bodies. In the latter scenario, the additional body could be a planet and is therefore crucial to understanding how these objects are formed and how they evolve around two parent stars. With the advent of large space missions, for example Kepler and TESS (Transiting Exoplanet Survey Satellite), an enormous amount of high precision photometric data with temporal coverage from years to decades has become available. Thus, in this work we propose to study the orbital period variation of a sample of 240 binary systems that was observed by the Kepler and TESS and, therefore, with a temporal coverage of more than 14 years. The main goal of this paper is the search and characterization of third bodies, however, all phenomena that generate the variation of the orbital period of binary systems will be investigated. Out of the sample of 240 binary star systems, 78 of them showed cyclic variation in the their O-C diagrams and 162 of them have non-cyclic variation in the O-C diagram detected.

Keywords: Exoplanets (498) — Multiple stars (1081) — Eclipsing binary stars (444) — Variable star period change (1760)

1. INTRODUCTION

Binary stars, which consist of two stars orbiting a common center of mass, have contributed richly to several areas in Astrophysics (e.g., Sana et al. 2012; Grun-
dahl et al. 2008; Clausen et al. 2008). A sub-
class of these systems, the eclipsing binaries, which have
their orbital planes in the observer’s line of sight and
therefore eclipse each other, are used to determine dis-
tances, and calculate fundamental parameters of stars
(e.g. mass and radii) to test models of stellar evolution
(e.g., Pietrzyński et al. 2012; Almeida et al. 2015, 2017).

Another topic of fundamental importance on eclipsing binary systems is the study of orbital period variation. They are used to understand various physical phenomena, e.g. emission of gravitational waves (Hulse & Taylor 1975), loss of angular momentum via mag-
netic braking (Tout & Hall 1991), transfer of matter be-
tween components (Tout & Hall 1991; Cehula & Pejcha
2023), apsidal motion (Gimenez & Garcia-Pelayo 1983),

⁴³ variation of quadrupole momentum (Applegate & Pat-
⁴⁴ terson 1987) and the presence of circumbinary bodies
⁴⁵ (Correia et al. 2016). In the latter scenario, the addi-
⁴⁶ tional bodies could be planets, and therefore, crucial to
⁴⁷ understand how these objects are formed and how they
⁴⁸ evolve around two parent stars (Martin & Triaud 2015).

⁴⁹ The characterization of binary, triple or higher order
⁵⁰ systems becomes crucial for us to understand several
⁵¹ stellar physical processes, e.g. Tidal friction, Kozai cy-
⁵² cles, mass transfer, angular momentum loss, merging
⁵³ (Tokovinin et al. 2006; Tokovinin 1997; Sana & Evans
⁵⁴ 2010; Duchêne & Kraus 2013; Sana 2016), which we
⁵⁵ would not be able to observe in isolated stars. Fur-
⁵⁶ thermore, we know that the way to directly measure the
⁵⁷ mass of a star is through a binary system.

⁵⁸ Space missions, such as Kepler and TESS (*Transit-*
⁵⁹ *ting Exoplanet Survey Satellite*), have contributed signif-
⁶⁰ icantly to the discoveries of planets around single stars
⁶¹ and in multiple systems (e.g., Batalha et al. 2011;

⁶² Borucki 2016; Astudillo-Defru et al. 2020; Gандolfi et al. 2018). Kepler, launched by NASA (North American Space Agency), began its mission in 2009 and had as main scientific objective to detect exoplanets by the method of planetary transits, with emphasis on terrestrial planets ($R < 2.5R_{\oplus}$), located within the habitable zones of Sun-like stars (Borucki et al. 2010). To continue with the mission to discover exoplanets, the TESS space telescope was launched in 2018 by NASA, and it is still in full operation with the aim of searching for planets that transit bright stars and close to the our Solar system (Ricker et al. 2014).

Combining data from the Kepler and TESS satellites, with temporal coverage of more than 14 years of observation, provides an excellent opportunity to study long-term phenomena. In this context, this paper aims to study the orbital period variation of the eclipsing binary systems observed by the Kepler and TESS satellites. To do so, we selected a sample of 240 eclipsing binary systems reported by Conroy et al. (2014) with data of both missions. The analysis of the orbital period variation of these systems will be done through the O-C (Observed minus Calculated) diagrams, see e.g. (Conroy et al. 2014; Almeida et al. 2019), and classified in cyclic and non-cyclic variations. For the systems with cyclic variations, it will be investigated if additional bodies can explain their O-C diagrams.

This paper is organized as follow. The Section 2 we present the data used for our study and data processing. In Section 3 we present the determination of the period of the binary system, the construction of phase diagram, the determination of the eclipse times, and the adjustment for the third body in our data. Finally, in Section 4 we present the results of this study and discuss them in Section 5.

2. SAMPLE SELECTION AND DATA PROCESSING

For this study, we use a sample of 240 binary systems selected out of 1279 targets reported by Conroy et al. (2014). The selection criterion was that the binaries have been observed by the Kepler and TESS satellites. Combining both data set, the temporal baseline of observations for all targets is more than 14 years. In Table 1, we list all targets with the inner binary's orbital period, eccentricity and orbital period of the third body reported by Conroy et al. (2014).

As we can see in Table 1, for some targets, e.g. KIC 3221207 and KIC 3936357, due to the relatively short temporal coverage of Kepler data, considering the long-term variations of the possible third bodies, Conroy

Table 1. Inner binary orbital period (P_{bin}), orbital period (P_3) and eccentricity (e_3) of the third body derived by Conroy et al. (2014).

KIC	P_{bin}	P_3	e_3
	days	days	
2450566	1.845	983.7 ± 472.8	0.308 ± 0.016
3221207	0.474	~ 1700	
3228863	0.731	644.1 ± 15.7	0.000 ± 0.003
3641446	2.100	228.6 ± 1.0	0.000 ± 0.010
3936357	0.369	~ 2400	

NOTE—Table 1 is published in its entirety in the machine-readable format.

¹¹¹ et al. (2014) do not provide the values for their eccentricities.

¹¹³ To search and download the Kepler and TESS light curves from the MAST webpage¹, we used the ¹¹⁴ **Lightkurve** python package (Lightkurve Collaboration ¹¹⁵ et al. 2018). The presearch data conditioned simple ¹¹⁶ aperture photometry (PDCSAP) flux from both Kepler ¹¹⁷ and TESS satellites have been chosen for our analysis. The PDCSAP pipeline try to remove systematic ¹¹⁸ effects, e.g. long-term trends, discontinuities within the ¹¹⁹ quarters, etc. For our sample, Kepler data are available in long cadence (30 minutes), while TESS data are ¹²⁰ available in long (30 minutes) and short (2 minutes) ¹²¹ cadences. For our propose, due to best temporal precision, ¹²² we use the TESS short cadence data.

¹²³ Additional steps for the light curve preparation ¹²⁴ were done. We use the **flatten** function from ¹²⁵ **Lightkurve** to remove the low frequency trend using the ¹²⁶ **Savitzky-Golay** filter from Scipy package and normalize ¹²⁷ the light curve. Besides, the **remove_outliers** function ¹²⁸ from **Lightkurve** which removes the outliers points ¹²⁹ from the light curves based on the **sigma-clipping** algorithm ¹³⁰ were used.

3. DATA ANALYSIS

¹³⁴ The main goal of this paper is searching for variations ¹³⁵ in the O-C diagram of our selected binaries that could ¹³⁶ indicate third bodies around them. To do so, we perform ¹³⁷ the following steps: (i) determine the orbital period ¹³⁸ of the system and build its phase diagram; (ii) perform ¹³⁹ a Polyfit adjustment to obtain the eclipse instants and ¹⁴⁰ build the O-C diagram via a linear ephemeris; and (iii)

¹ <https://archive.stsci.edu/>

analyze the binary orbital period variation using the O-C diagram. These steps are done in the following sections.

3.1. Period determination and phase diagram construction

As the Kepler and TESS data are not uniformly spaced in time, see Figure 1, to determine the binary orbital period, the Lomb-Scargle (LS) method (Lomb 1976; Scargle 1982) was used via `Lightkurve` program. Figure 2 shows the LS periodogram for the KIC 5513861 (TIC 120251815) system.

Having determined the period of the system, Fig. 2, we use the `stringlength` tool (Dworetsky 1983), a method of `pyTiming` from the PyAstronomy² library (Czesla et al. 2019), for a refinement of the obtained period. This method is suitable for non-sinusoidal periodic variations, e.g. eclipsing binaries, planetary transit, etc, returning as output the sum of the lengths among the points measured in the phase diagram, which is constructed for a period grid, see Fig. 3. The minimum output value gives the best period for the data considering the searched range.

Finally, we phase the light curve using the period of the binary system calculated in the previous step. To construct the phase diagram, we use the `fold` command of the `Lightkurve` program. The result for KIC 5513861 system is shown in Figure 4.

3.2. Determining the period variations

To determine the eclipse times of our close binary sample, we perform the same procedure done by Conroy et al. (2014). In short, the phased light curves of the binary systems are divided in four parts and each one is fitted by a chain of nth-order polynomial $P(x)$, as described in Prša et al. (2008). The fitting procedure is done using a computational algorithm called `Polyfit` which is available by Prša et al. (2008). This code is based on two principles: (i) $P(x)$ differentiable at nodes is not required, it allows to break the polynomial chain, and (ii) the nodes can change their positions iteratively driving the solution to the nearest minimum.

In our analysis, we adopt a 2nd order polynomial with 10000 iterations and step of 0.04 in phase for the search of each node. Thus, four polynomial solutions were derived and added to provide the general solution for the phased light curve, see one example in Fig 4. With respect to this last solution, we calculate the phase shift in each cycle of the binary, which multiplied by the orbital period gives the O-C diagram, see Fig. 7. A detailed

and complete description of the algorithm is available at Prša et al. (2008).

3.3. Search for periodic signal in the O-C Diagram

With the O-C diagram of our sample in hand, the next step is to search for periodic variations that may indicate possible additional components gravitationally interacting with the binary. To do this, we apply the same procedure as done in Section 3.1. To consider a reliable period, we adopted frequencies in the Lomb-Scargle periodogram above 10% of false alarm probability. As an example, Figure 5 shows the Lomb-Scargle periodogram generated from the O-C diagram data of KIC 5513861. In total, 78 of the 240 binaries analyzed show significant variations in their orbital period. These systems will be analyzed in the context of light travel time in the next section.

4. RESULTS

By analyzing the light curves of our sample of 240 close binary stars, we obtained a total of 78 systems that showed periodic variation in their O-C diagrams. For these binaries, we analyse the period variation in the context of a third component gravitationally interacting with the inner binary, see Section 4.1.

The remaining 162 objects, we do not identify any significant periodic variations, see one example in Figure 6. All results for these systems are reported in Appendix B. The analysis and discussion of the possible causes for these binaries are beyond the scope of this paper and, therefore, will be carried out in future work.

4.1. Light Travel Time Effect

The Light Travel Time (LTT) effect is caused by the presence of an invisible body gravitationally interacting with an object of interest, in our case a close binary system, and consists of periodic variations in the arriving time of a periodic intrinsic signal, e.g. eclipsing times, from the binary.

The variation caused by the LTT effect in the binary orbital period, can be mathematically described as follows (Irwin 1952):

$$\tau = \frac{a \sin i}{c} \frac{1 - e^2}{1 + e \cos f} \sin(f + \omega), \quad (1)$$

where a is the semi-major axis, e is the eccentricity, i is the orbital inclination with respect to the plane of the sky, ω is the periastron argument, f is the true anomaly, and c the speed of light.

In addition to the LTT effect, the O-C diagram of some of these systems showed long-term changes in their orbital period. Thus, for such systems, we added a linear

² <https://github.com/sczesla/PyAstronomy>

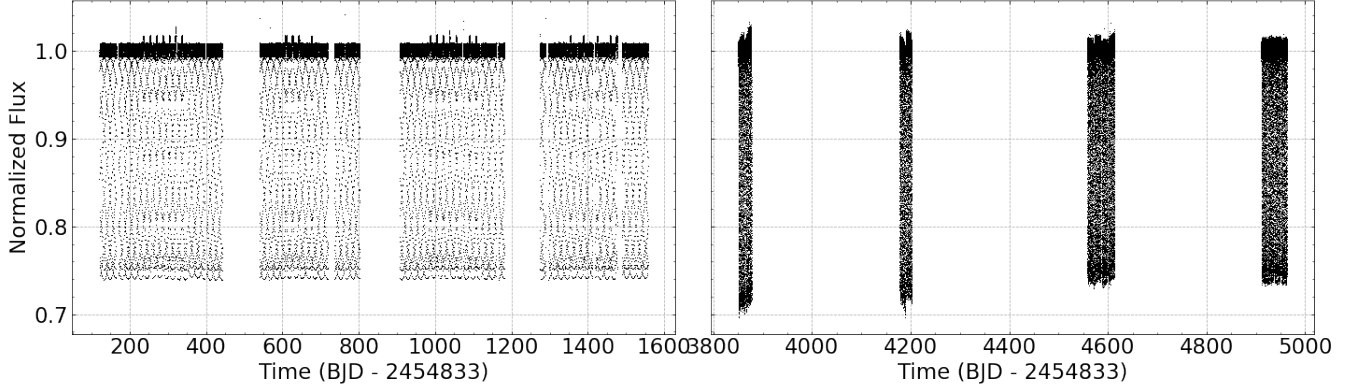


Figure 1. Normalized light curve from Kepler data (left panel) and TESS data (right panel) of KIC 5513861 (TIC 120251815).

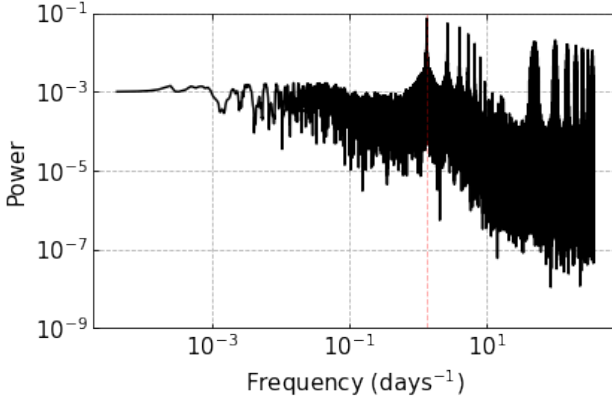


Figure 2. Lomb-Scargle periodogram obtained from the KIC 5513861 light curve. Vertical red dashed line shows the frequency with highest power.

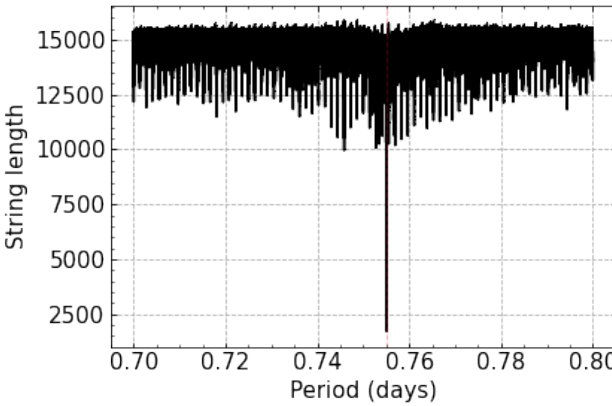


Figure 3. Stringlength periodogram used to refine the period determination of the KIC 5513861 object. Vertical red dashed line shows the period with lower string length.

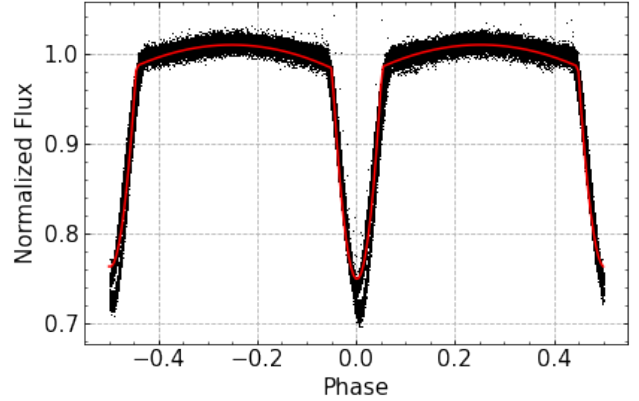


Figure 4. Phase diagram of KIC 5513861. Red line represent the best solution derived by the Polyfit program.

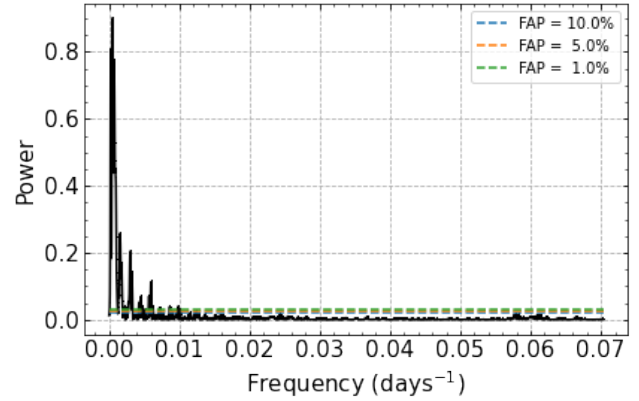


Figure 5. Lomb-scargle Periodogram of the O-C diagram data of KIC 5513861. The green, orange and blue dashed lines indicate 1%, 5% and 10% for the false alarm probability levels, respectively.

²³⁷ term to Eq. 1 to fit the data and obtain the general
²³⁸ solution, as illustrated in Fig. 8.

²³⁹ The fitting procedure were done in two steps. Initially,
²⁴⁰ to find a preliminary solution, the Optimize Curve Fit

²⁴¹ task from SciPy library were executed. In the second
²⁴² step, we run a Markov Chain Monte Carlo (MCMC) pro-
²⁴³cedure through emcee program (Foreman-Mackey et al.
²⁴⁴ 2013), using the preliminary solution as a initial guess,

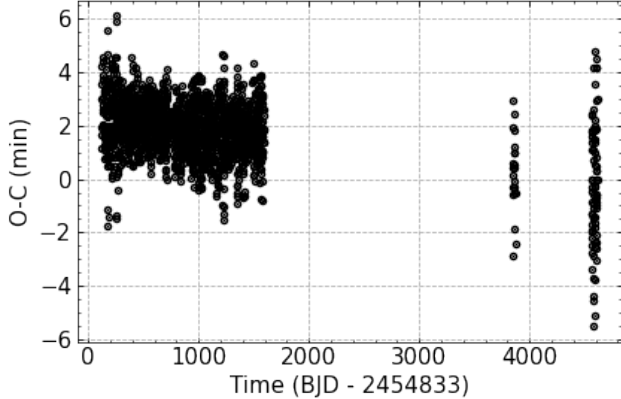


Figure 6. O-C diagram for the binary system KIC 1868650 (TIC 137306463).

to obtain the final solution, as well as, the error bars in each fitted parameter. Figures 7 and 8 show two results of our fitting procedure, the first with only the LTT curve and the second with the addition of the linear term. All results for the 78 systems with periodic variations are presented in Section A and the fitted parameters are listed in Table 2.

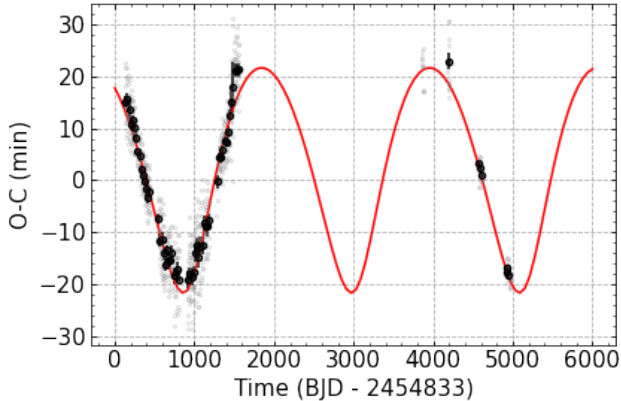


Figure 7. O-C diagram for the binary system KIC 5513861 (TIC 120251815). Individual and average of 20 measurements are shown with gray and black points, respectively. The red curve represents the best fit considering a third body around the inner binary.

5. DISCUSSIONS

Our sample of 240 close binaries were divided into two main groups: (1) systems with periodic variations in their O-C diagrams, which were fitted with an LTT curve or an LTT curve plus a linear function, and (2) systems with non-cyclic variation, which are defined as those that despite having short, increasing, decreasing or random variations in their O-C diagrams, such vari-

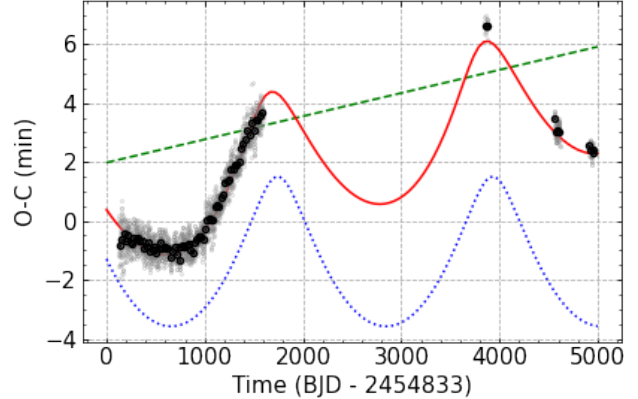


Figure 8. O-C diagram for the binary system KIC 3221207 (TIC 121213501). Individual and average of 20 measurements are shown with gray and black points. The red curve is the best solution obtained when used the sum of the LTT effect (dotted blue curve) plus the linear term (dashed green line).

ations do not have an associated period with statistical significance according to the FAP.

Following the same criteria adopted by Conroy et al. (2014), we divided our sample with periodic variations into 3 subgroups according to the periods found in the O-C diagrams and the temporal baseline of the Kepler and TESS data: objects with (i) periods less than 2400 days ($P < 2400$ days), (ii) periods greater or equal than 2400 and less or equal than 4800 days ($2400 \leq P(\text{days}) \leq 4800$), and (iii) periods greater than 4800 days ($P > 4800$ days). We obtained 47, 16 and 15 systems for these three subgroups, respectively. Table 2 shows these systems according to this classification and the orbital periods and eccentricities for the third body candidates.

Table 2. Binary systems with periodic variations in their O-C diagrams. The targets are divided in three intervals: periods less than 2400 days, between 2400 and 4800 days, and greater than 4800 days.

KIC	P_3	e_3	timebase
	days		
2450566	$1059.282^{+23.443}_{-28.695}$	$0.655^{+0.105}_{-0.066}$	3757
2708156	$1437.154^{+13.913}_{-7.553}$	$0.087^{+0.167}_{-0.065}$	4870
3221207	$2253.652^{+72.383}_{-62.009}$	$0.426^{+0.048}_{-0.040}$	4840
3228863	$663.632^{+6.202}_{-15.304}$	$0.224^{+0.173}_{-0.154}$	4870
3641446	$331.383^{+45.999}_{-38.847}$	$0.930^{+0.041}_{-0.066}$	3760

Table 2 *continued*

Table 2 (continued)

KIC	P_3	e_3	timebase
	days		
3936357	2132.636 ^{+67.619} _{-47.151}	0.120 ^{+0.075} _{-0.061}	4840
4451148	769.411 ^{+6.770} _{-10.758}	0.466 ^{+0.087} _{-0.023}	4840
4647652	755.235 ^{+19.495} _{-13.418}	0.245 ^{+0.290} _{-0.147}	4870
4909707	513.727 ^{+0.617} _{-0.517}	0.657 ^{+0.029} _{-0.027}	4840
4945588	1607.893 ^{+29.331} _{-140.789}	0.871 ^{+0.046} _{-0.045}	4870
4999260	2118.002 ^{+60.654} _{-33.107}	0.717 ^{+0.036} _{-0.032}	4870
5022573	1826.598 ^{+113.755} _{-113.477}	0.766 ^{+0.083} _{-0.061}	3760
5264818	282.272 ^{+2.898} _{-4.298}	0.436 ^{+0.208} _{-0.309}	4870
5513861	2113.335 ^{+5.927} _{-6.342}	0.315 ^{+0.019} _{-0.029}	4840
5975712	1694.123 ^{+2.155} _{-1.001}	0.218 ^{+0.001} _{-0.001}	3780
6187893	2028.925 ^{+5.819} _{-5.788}	0.969 ^{+0.004} _{-0.006}	4840
6205460	2311.862 ^{+83.952} _{-29.020}	0.426 ^{+0.019} _{-0.071}	4870
7375612	2123.456 ^{+15.279} _{-7.569}	0.098 ^{+0.074} _{-0.028}	4870
7385478	1360.065 ^{+76.397} _{-101.476}	0.782 ^{+0.148} _{-0.363}	4870
7431703	1820.383 ^{+42.684} _{-105.177}	0.448 ^{+0.121} _{-0.158}	4870
7440742	2003.253 ^{+133.920} _{-126.183}	0.983 ^{+0.005} _{-0.013}	4870
7765894	463.815 ^{+3.584} _{-5.356}	0.270 ^{+0.073} _{-0.088}	4870
7766185	1860.287 ^{+99.837} _{-87.249}	0.945 ^{+0.015} _{-0.024}	4870
7816201	2328.001 ^{+209.934} _{-397.908}	0.696 ^{+0.074} _{-0.124}	4840
7938870	2100.595 ^{+31.818} _{-32.686}	0.627 ^{+0.094} _{-0.022}	4840
8043961	422.710 ^{+1.645} _{-1.526}	0.399 ^{+0.185} _{-0.121}	4870
8045121	890.971 ^{+14.033} _{-17.999}	0.349 ^{+0.085} _{-0.122}	3785
8231231	1909.021 ^{+50.390} _{-54.438}	0.949 ^{+0.021} _{-0.033}	3785
8285349	2042.641 ^{+16.160} _{-55.476}	0.522 ^{+0.022} _{-0.218}	4870
8386865	294.267 ^{+0.998} _{-0.874}	0.421 ^{+0.055} _{-0.033}	3785
8579707	1944.760 ^{+203.672} _{-24.784}	0.523 ^{+0.090} _{-0.037}	4870
9083523	2200.587 ^{+36.070} _{-16.377}	0.370 ^{+0.084} _{-0.090}	4870
9181877	1830.374 ^{+20.089} _{-49.420}	0.596 ^{+0.054} _{-0.051}	4870
9365025	731.626 ^{+3.616} _{-2.190}	0.969 ^{+0.002} _{-0.003}	3785
9402652	1499.321 ^{+2.076} _{-2.039}	0.817 ^{+0.028} _{-0.034}	4870
9451096	100.092 ^{+0.068} _{-0.086}	0.998 ^{+0.001} _{-0.001}	4870
9657096	1829.705 ^{+96.740} _{-26.635}	0.607 ^{+0.034} _{-0.077}	3785
10226388	924.443 ^{+9.411} _{-1.880}	0.518 ^{+0.238} _{-0.031}	4900
10389982	2300.442 ^{+103.102} _{-37.377}	0.839 ^{+0.111} _{-0.090}	4870
10724533	1936.467 ^{+52.152} _{-28.855}	0.426 ^{+0.035} _{-0.185}	4870
10789421	455.994 ^{+10.275} _{-18.197}	0.517 ^{+0.281} _{-0.180}	4870
10818544	1892.800 ^{+120.088} _{-78.434}	0.967 ^{+0.011} _{-0.030}	3785
10979669	1532.272 ^{+54.987} _{-20.992}	0.974 ^{+0.008} _{-0.013}	4870
10991989	611.634 ^{+1.753} _{-1.898}	0.977 ^{+0.011} _{-0.057}	4900
11572643	2290.326 ^{+48.331} _{-46.637}	0.503 ^{+0.314} _{-0.198}	4900

Table 2 continued**Table 2** (continued)

KIC	P_3	e_3	timebase
	days		
12216817	1508.869 ^{+27.582} _{-41.085}	0.619 ^{+0.071} _{-0.084}	3785
12305537	2039.912 ^{+9.942} _{-11.011}	0.736 ^{+0.086} _{-0.038}	4900
3953981	2862.477 ^{+94.503} _{-122.901}	0.223 ^{+0.095} _{-0.069}	4870
4450976	2546.115 ^{+161.201} _{-203.502}	0.313 ^{+0.150} _{-0.201}	3760
4758368	2478.732 ^{+135.001} _{-129.068}	0.973 ^{+0.014} _{-0.080}	4870
4851217	2473.632 ^{+318.289} _{-147.137}	0.876 ^{+0.083} _{-0.056}	4870
6353203	2449.628 ^{+19.370} _{-7.118}	0.575 ^{+0.057} _{-0.069}	4870
7259917	4729.394 ^{+441.635} _{-196.787}	0.720 ^{+0.063} _{-0.222}	4840
7690843	2714.623 ^{+60.236} _{-72.170}	0.752 ^{+0.058} _{-0.152}	4870
7950962	3085.157 ^{+100.353} _{-116.633}	0.075 ^{+0.053} _{-0.055}	4870
8189196	3903.002 ^{+24.689} _{-30.698}	0.980 ^{+0.003} _{-0.004}	4870
8758161	2942.195 ^{+187.072} _{-137.064}	0.688 ^{+0.088} _{-0.170}	4870
9345838	2497.096 ^{+5.248} _{-7.119}	0.969 ^{+0.013} _{-0.009}	4870
9760531	2984.870 ^{+23.366} _{-31.904}	0.960 ^{+0.006} _{-0.095}	4870
10155563	3569.345 ^{+16.637} _{-16.118}	0.989 ^{+0.001} _{-0.002}	4840
10259530	4636.848 ^{+95.939} _{-92.547}	0.561 ^{+0.028} _{-0.173}	4870
10481912	4101.691 ^{+96.134} _{-510.167}	0.353 ^{+0.138} _{-0.120}	4900
11255667	4715.408 ^{+411.622} _{-203.023}	0.269 ^{+0.112} _{-0.143}	4870
3448245	8314.481 ^{+297.994} _{-89.964}	0.753 ^{+0.051} _{-0.014}	4870
4909422	6582.935 ^{+927.321} _{-1415.082}	0.839 ^{+0.131} _{-0.096}	4840
5296877	4962.088 ^{+11.012} _{-16.105}	0.728 ^{+0.010} _{-0.007}	4870
6462057	4926.320 ^{+359.711} _{-147.307}	0.637 ^{+0.080} _{-0.177}	4870
7457163	6255.520 ^{+135.002} _{-193.789}	0.527 ^{+0.062} _{-0.039}	4870
7512381	6805.413 ^{+249.021} _{-135.070}	0.411 ^{+0.040} _{-0.131}	4870
8397460	8112.505 ^{+509.919} _{-443.186}	0.966 ^{+0.003} _{-0.003}	4870
8587792	5493.004 ^{+294.492} _{-278.158}	0.380 ^{+0.046} _{-0.040}	4870
8894630	7635.890 ^{+351.320} _{-315.610}	0.737 ^{+0.043} _{-0.030}	4870
9602595	6556.627 ^{+175.520} _{-624.070}	0.762 ^{+0.037} _{-0.028}	4870
9612468	7444.129 ^{+487.713} _{-417.057}	0.620 ^{+0.044} _{-0.051}	3785
9832227	6091.433 ^{+142.763} _{-115.053}	0.507 ^{+0.028} _{-0.047}	4870
10485137	5843.721 ^{+412.625} _{-144.971}	0.639 ^{+0.072} _{-0.064}	4900
10711938	6688.888 ^{+261.034} _{-315.892}	0.631 ^{+0.250} _{-0.059}	4080
11409673	5483.304 ^{+199.637} _{-143.780}	0.972 ^{+0.009} _{-0.011}	4870

Table 3 present a comparison between our results with those from Conroy et al. (2014). In this table, we divided the systems with the same range of period variations as adopted by the last authors, i.e., $P < 700$ days, ($700 \leq P(\text{days}) < 1400$), and $P > 1400$ days. In these three ranges, we and Conroy et al. (2014) found: (i) 11 and 9 systems; (ii) 10 and 9 systems, and (iii) 57 and 16 systems, respectively. This results is illustrated in

Figure 9. Thus, as expected by adding TESS data and increasing the observational baseline, we found 78 close binaries with third body candidates, 2.3 times more systems than Conroy et al. (2014) in the sample of 240 systems. This result represents a rate of $\sim 33\%$ in our sample of close binaries. It is also important to note that most of the new systems found in this study are in the range of $P > 1400$ days.

When considering the number of cycles for the third body candidates observed in the data, Conroy et al. (2014) found 9 systems with at least two cycles, 9 with

at least one cycle and 16 targets with less than one cycle, while in this study we found 47, 16 and 15 systems for same ranges, respectively.

In addition to new systems with periodic variations in their orbital periods, with the combined data from Kepler and TESS and using the MCMC procedure, we were able to better estimate the parameters of the third body candidates, such as, for example, orbital periods and eccentricities. Table 3 summarises these parameters obtained in our fit in comparison with those from Conroy et al. (2014).

Table 3. Comparison between results of period and eccentricity for the third body candidates found in this paper (P_3 and e_3) and in Conroy et al. (2014) ($P_{3,C}$ and $e_{3,C}$).

KIC	P_3	$P_{3,C}$	e_3	$e_{3,C}$	base
	days	days			
3228863	$663.632^{+6.202}_{-15.304}$	644.1 ± 15.7	$0.224^{+0.173}_{-0.154}$	0.000 ± 0.003	4870
3641446	$331.383^{+45.999}_{-38.847}$	228.6 ± 1.0	$0.930^{+0.041}_{-0.066}$	0.000 ± 0.010	3760
4909707	$513.727^{+0.617}_{-0.517}$	516.1 ± 16.1	$0.657^{+0.029}_{-0.027}$	0.000 ± 0.010	4840
5264818	$282.272^{+2.898}_{-4.298}$	299.7 ± 107.5	$0.436^{+0.208}_{-0.309}$	0.421 ± 0.306	4870
7690843	$2714.623^{+60.236}_{-72.170}$	74.1 ± 0.1	$0.752^{+0.058}_{-0.152}$	0.233 ± 0.021	4870
7765894	$463.815^{+3.584}_{-5.356}$...	$0.270^{+0.073}_{-0.088}$...	4870
8043961	$422.710^{+1.645}_{-1.526}$	478.0 ± 10.4	$0.399^{+0.185}_{-0.121}$	0.000 ± 0.005	4870
8386865	$294.267^{+0.998}_{-0.874}$	293.9 ± 2.8	$0.421^{+0.055}_{-0.033}$	0.493 ± 0.013	3785
9451096	$100.092^{+0.068}_{-0.086}$	106.8 ± 0.1	$0.998^{+0.001}_{-0.001}$	0.091 ± 0.033	4870
10789421	$455.994^{+10.275}_{-18.197}$...	$0.517^{+0.281}_{-0.180}$...	4870
10991989	$611.634^{+1.753}_{-1.898}$	554.8 ± 64.1	$0.977^{+0.011}_{-0.057}$	0.000 ± 0.018	4900
2450566	$1059.282^{+23.443}_{-28.695}$	983.7 ± 472.8	$0.655^{+0.105}_{-0.066}$	0.308 ± 0.016	3757
4451148	$769.411^{+6.770}_{-10.758}$	746.0 ± 52.1	$0.466^{+0.087}_{-0.023}$	0.293 ± 0.004	4840
4647652	$755.235^{+19.495}_{-13.418}$	755.2 ± 44.3	$0.245^{+0.290}_{-0.147}$	0.244 ± 0.003	4870
5975712	$1694.123^{+2.155}_{-1.001}$	1164.7 ± 964.3	$0.218^{+0.001}_{-0.001}$	0.000 ± 0.013	3780
7385478	$1360.065^{+76.397}_{-101.476}$	1389.3 ± 795.2	$0.782^{+0.148}_{-0.363}$	0.245 ± 0.007	4870
8045121	$890.971^{+14.033}_{-17.999}$	938.6 ± 25.8	$0.349^{+0.085}_{-0.122}$	0.000 ± 0.001	3785
9365025	$731.626^{+3.616}_{-2.190}$...	$0.969^{+0.002}_{-0.003}$...	3785
9612468	$7444.129^{+487.713}_{-417.057}$	1264.2 ± 233.2	$0.620^{+0.044}_{-0.051}$	0.340 ± 0.001	3785
10226388	$924.443^{+9.411}_{-1.880}$	965.3 ± 183.8	$0.518^{+0.238}_{-0.031}$	0.041 ± 0.007	4900
10724533	$1936.467^{+52.152}_{-28.855}$	1131.4 ± 197.7	$0.426^{+0.035}_{-0.185}$	0.265 ± 0.003	4870
2708156	$1437.154^{+13.913}_{-7.553}$...	$0.087^{+0.167}_{-0.065}$...	4870
3221207	$2253.652^{+72.383}_{-62.009}$	~ 1700	$0.426^{+0.048}_{-0.040}$...	4840
3448245	$8314.481^{+297.994}_{-89.964}$...	$0.753^{+0.051}_{-0.014}$...	4870
3936357	$2132.636^{+67.619}_{-47.151}$	~ 2400	$0.120^{+0.075}_{-0.061}$...	4840
3953981	$2862.477^{+94.503}_{-122.901}$...	$0.223^{+0.095}_{-0.069}$...	4870
4450976	$2546.115^{+161.201}_{-203.502}$...	$0.313^{+0.150}_{-0.201}$...	3760

Table 3 *continued*

Table 3 (*continued*)

KIC	P_3	$P_{3,C}$	e_3	$e_{3,C}$	base
	days	days			
4758368	2478.732^{+135.001}_{-129.068}	~ 1500	0.973^{+0.014}_{-0.080}	...	4870
4851217	2473.632 ^{+318.289} _{-147.137}	...	0.876 ^{+0.083} _{-0.056}	...	4870
4909422	6582.935 ^{+927.321} _{-1415.082}	...	0.839 ^{+0.131} _{-0.096}	...	4840
4945588	1607.893 ^{+29.331} _{-140.789}	~ 1500	0.871 ^{+0.046} _{-0.045}	...	4870
4999260	2118.002 ^{+60.654} _{-33.107}	...	0.717 ^{+0.036} _{-0.032}	...	4870
5022573	1826.598 ^{+113.755} _{-113.477}	...	0.766 ^{+0.083} _{-0.061}	...	3760
5296877	4962.088 ^{+11.012} _{-16.105}	~ 1900	0.728 ^{+0.010} _{-0.007}	...	4870
5513861	2113.335 ^{+5.927} _{-6.342}	~ 1800	0.315 ^{+0.019} _{-0.029}	...	4840
6187893	2028.925 ^{+5.819} _{-5.788}	~ 7800	0.969 ^{+0.004} _{-0.006}	...	4840
6205460	2311.862 ^{+83.952} _{-29.020}	...	0.426 ^{+0.019} _{-0.071}	...	4870
6353203	2449.628 ^{+19.370} _{-7.118}	...	0.575 ^{+0.057} _{-0.069}	...	4870
6462057	4926.320 ^{+359.711} _{-147.307}	...	0.637 ^{+0.080} _{-0.177}	...	4870
7259917	4729.394 ^{+441.635} _{-196.787}	...	0.720 ^{+0.063} _{-0.222}	...	4840
7375612	2123.456 ^{+15.279} _{-7.569}	~ 2100	0.098 ^{+0.074} _{-0.028}	...	4870
7431703	1820.383 ^{+42.684} _{-105.177}	...	0.448 ^{+0.121} _{-0.158}	...	4870
7440742	2003.253 ^{+133.920} _{-126.183}	...	0.983 ^{+0.005} _{-0.013}	...	4870
7457163	6255.520 ^{+135.002} _{-193.789}	...	0.527 ^{+0.062} _{-0.039}	...	4870
7512381	6805.413 ^{+249.021} _{-135.070}	...	0.411 ^{+0.040} _{-0.131}	...	4870
7766185	1860.287 ^{+99.837} _{-87.249}	...	0.945 ^{+0.015} _{-0.024}	...	4870
7816201	2328.001 ^{+209.934} _{-397.908}	...	0.696 ^{+0.074} _{-0.124}	...	4840
7938870	2100.595 ^{+31.818} _{-32.686}	...	0.627 ^{+0.094} _{-0.022}	...	4840
7950962	3085.157 ^{+100.353} _{-116.633}	...	0.075 ^{+0.053} _{-0.055}	...	4870
8189196	3903.002 ^{+24.689} _{-30.695}	~ 8300	0.980 ^{+0.003} _{-0.004}	...	4870
8231231	1909.021 ^{+50.390} _{-54.438}	~ 1600	0.949 ^{+0.021} _{-0.033}	...	3785
8285349	2042.641 ^{+16.160} _{-55.476}	...	0.522 ^{+0.022} _{-0.218}	...	4870
8397460	8112.505 ^{+509.919} _{-443.186}	...	0.966 ^{+0.003} _{-0.003}	...	4870
8579707	1944.760 ^{+203.672} _{-24.784}	...	0.523 ^{+0.090} _{-0.037}	...	4870
8587792	5493.004 ^{+294.492} _{-278.158}	...	0.380 ^{+0.046} _{-0.040}	...	4870
8758161	2942.195 ^{+187.072} _{-137.064}	...	0.688 ^{+0.088} _{-0.170}	...	4870
8894630	7635.890 ^{+351.320} _{-315.610}	...	0.737 ^{+0.043} _{-0.030}	...	4870
9083523	2200.587 ^{+36.070} _{-16.377}	~ 5200	0.370 ^{+0.084} _{-0.090}	...	4870
9181877	1830.374 ^{+20.089} _{-49.420}	~ 2600	0.596 ^{+0.054} _{-0.051}	...	4870
9345838	2497.096 ^{+5.248} _{-7.119}	...	0.969 ^{+0.013} _{-0.009}	...	4870
9402652	1499.321 ^{+2.076} _{-2.039}	...	0.817 ^{+0.028} _{-0.034}	...	4870
9602595	6556.627 ^{+175.520} _{-624.070}	...	0.762 ^{+0.037} _{-0.028}	...	4870
9657096	1829.705 ^{+96.740} _{-26.635}	~ 1400	0.607 ^{+0.034} _{-0.077}	...	3785
9760531	2984.870 ^{+23.366} _{-31.904}	...	0.960 ^{+0.006} _{-0.095}	...	4870
9832227	6091.433 ^{+142.763} _{-115.053}	...	0.507 ^{+0.028} _{-0.047}	...	4870
10155563	3569.345 ^{+16.637} _{-16.118}	...	0.989 ^{+0.001} _{-0.002}	...	4840
10259530	4636.848 ^{+95.939} _{-92.547}	...	0.561 ^{+0.028} _{-0.173}	...	4870

Table 3 *continued*

Table 3 (*continued*)

KIC	P_3	$P_{3,C}$	e_3	$e_{3,C}$	base
	days	days			
10389982	$2300.442^{+103.102}_{-37.377}$...	$0.839^{+0.111}_{-0.090}$...	4870
10481912	$4101.691^{+96.134}_{-510.167}$	~ 2700	$0.353^{+0.138}_{-0.120}$...	4900
10485137	$5843.721^{+412.625}_{-144.971}$	~ 3100	$0.639^{+0.072}_{-0.064}$...	4900
10711938	$6688.888^{+261.034}_{-315.892}$	~ 2000	$0.631^{+0.250}_{-0.059}$...	4080
10818544	$1892.800^{+120.088}_{-78.434}$...	$0.967^{+0.011}_{-0.030}$...	3785
10979669	$1532.272^{+54.987}_{-20.992}$...	$0.974^{+0.008}_{-0.013}$...	4870
11255667	$4715.408^{+411.622}_{-203.023}$...	$0.269^{+0.112}_{-0.143}$...	4870
11409673	$5483.304^{+199.637}_{-143.780}$...	$0.972^{+0.009}_{-0.011}$...	4870
11572643	$2290.326^{+48.331}_{-46.637}$...	$0.503^{+0.314}_{-0.198}$...	4900
12216817	$1508.869^{+27.582}_{-41.085}$...	$0.619^{+0.071}_{-0.084}$...	3785
12305537	$2039.912^{+9.942}_{-11.011}$...	$0.736^{+0.086}_{-0.038}$...	4900

305 Among the systems presented in Tables 2 and 3, there
 306 are 60 systems that do not have values defined in the
 307 Conroy et al. (2014) paper for a possible third body,
 308 and 16 of them have only an estimated value for the
 309 period of the third body.

310 The relationship between the periods of the inner bi-
 311 naries and the third body candidates measured in this
 312 paper and by Conroy et al. (2014) can be visualised in
 313 Fig. 9. There is no significant difference between our
 314 measurements and those carried out by Conroy et al.
 315 (2014) for the orbital period measurements of the inner

316 binaries. It is evident that $\sim 97\%$ of binaries with poten-
 317 tial third bodies have periods shorter than 4 days and
 318 that there is no presence of binary systems with peri-
 319 ods longer than 12 days ($P > 12$) with potential ter-
 320 tiary companions, consistent with results obtained by
 321 Tokovinin et al. (2006).

322 The website [https://projectc-production.up.railway.
 323 app/](https://projectc-production.up.railway.app/) provides the results for all close binaries, with and
 324 without periodic orbital variations, studied in the paper.

325 *Software:* polyfit (Prša et al. 2008), lightkurve
 326 (Lightkurve Collaboration et al. 2018), pyastronomy
 327 (Czesla et al. 2019), emcee (Foreman-Mackey et al.
 328 2013)

329

APPENDIX

330

331 Here, binary systems are listed by type of variation in their respective O-C diagrams. In Section B, those systems
 332 with non-periodic variations are presented; in Section A those with periodic variations. And, in Section C we present
 333 the full table with the orbital parameters found for those systems whose variations are periodic and non-periodic for
 334 our sample of 240 eclipsing binary systems.

335 A. BINARY SYSTEMS WITH PERIODIC VARIATIONS ON THE O-C DIAGRAM

336 Of the 240 binary systems in our sample, a total of 13 systems, 5.42% of the sample, have periodic variations shown
 337 in their O-C diagrams. In the following subsections we present each system with its respective characteristics for the
 338 possible third bodies orbiting its respective binary system. For each object we derive, by adjusting for a third body,
 339 its orbital period P , its eccentricity e , semi-major axis a and periastron argument ω .

340 A.1. KIC 2450566 (TIC 137977804) Object

341 This object presents a periodic variation in its O-C diagram, Fig. 11, intuiting the presence of a third body around
 342 the binary system with a period $P = 1059.282^{+23.443}_{-28.695}$, in an orbit with eccentricity $e = 0.655^{+0.105}_{-0.066}$, at a distance
 343 $a = 1487.083^{+181.846}_{-150.956}$ from its parent stars, with its inclination axis $\omega = 307.417^{+10.050}_{-17.567}$.

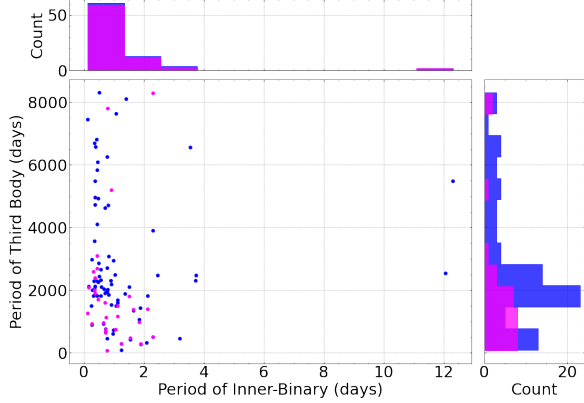


Figure 9. Period of the inner binary versus period of the third body candidates. The blue and magenta points represent our measurement and the results from Conroy et al. (2014), respectively. The top and left histograms represent the count of binaries and third body candidates in function of the their orbital periods, respectively.

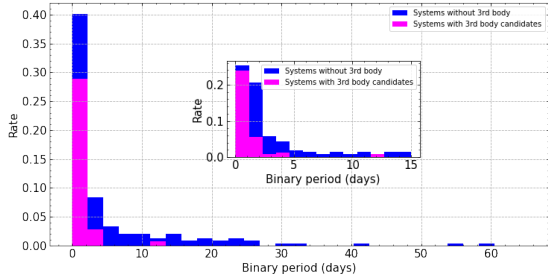


Figure 10.

A.2. KIC 2708156 (TIC 122375269) Object

This object presents a periodic variation in its O-C diagram, Fig. 12, intuiting the presence of a third body around the binary system with a period $P = 1460.490^{+2.093}_{-0.955}$, in an orbit with eccentricity $e = 0.396^{+0.001}_{-0.001}$, at a distance $a = 3690.709^{+2.778}_{-3.835}$ from its parent stars, with its inclination axis $\omega = 191.298^{+0.425}_{-0.554}$.

A.3. KIC 3221207 (TIC 121213501) Object

This object presents a periodic variation in its O-C diagram, Fig. 13, intuiting the presence of a third body around the binary system with a period $P = 2253.652^{+72.383}_{-62.009}$, in an orbit with eccentricity $e = 0.426^{+0.048}_{-0.040}$, at a distance $a = 413.398^{+17.810}_{-25.905}$ from its parent stars, with its inclination axis $\omega = 68.923^{+25.187}_{-29.382}$.

A.4. KIC 3228863 (TIC 394179296) Object

This object presents a periodic variation in its O-C diagram, Fig. 14, intuiting the presence of a third body around the binary system with a period $P = 663.632^{+6.202}_{-15.304}$, in an orbit with eccentricity $e = 0.224^{+0.173}_{-0.154}$, at a distance $a = 659.632^{+27.744}_{-56.636}$ from its parent stars, with its inclination axis $\omega = 260.622^{+23.252}_{-4.142}$.

A.5. KIC 3448245 (TIC 137687487) Object

This object presents a periodic variation in its O-C diagram, Fig. 15, intuiting the presence of a third body around the binary system with a period $P = 8314.481^{+297.994}_{-89.964}$, in an orbit with eccentricity $e = 0.753^{+0.051}_{-0.014}$, at a distance $a = 298.060^{+7.057}_{-5.386}$ from its parent stars, with its inclination axis $\omega = 0.860^{+2.637}_{-0.683}$.

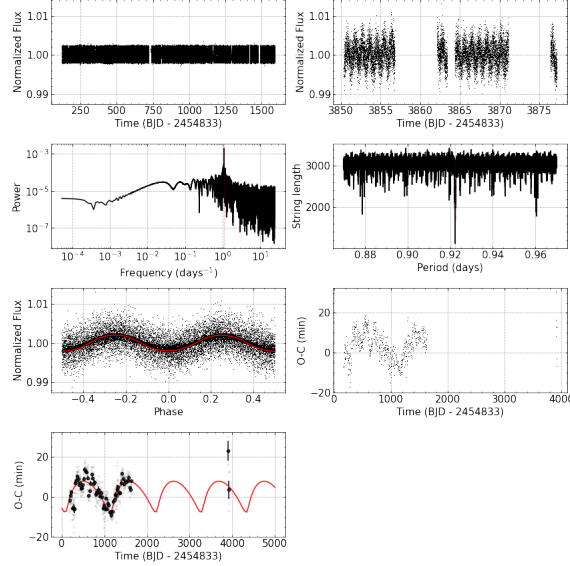


Figure 11. Analysis of objects KIC 2450566 (TIC 137977804). First row, left panel: Light curve from Kepler in terms of Normalized Flux over Time (BJD). Right panel: Light curve from TESS in terms of Normalized Flux over Time (BJD). Second row, left panel: Periodogram analysis to obtain the system's period. Right panel: String length to refine the obtained period. Third row, left panel: Light curve in phase - black points represent the data, and the red curve represents the best fit. Right panel: O-C diagram. Fourth row, left panel: O-C diagram with its curve adjusted for the presence of a third body; the gray points are the raw data points, the black points are the binned points, and the red curve represents the best fit for the third body around the eclipsing binary system.

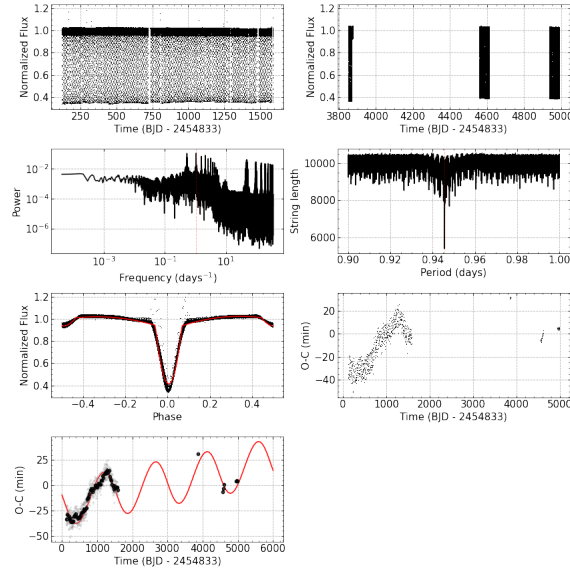


Figure 12. O-C diagram for the binary system KIC 2708156 (TIC 122375269).

A.6. KIC 3641446 (TIC 122303843) Object

This object presents a periodic variation in its O-C diagram, Fig. 16, intuiting the presence of a third body around the binary system with a period $P =$, in an orbit with eccentricity $e =$, at a distance $a =$ from its parent stars, with its inclination axis $\omega =$.

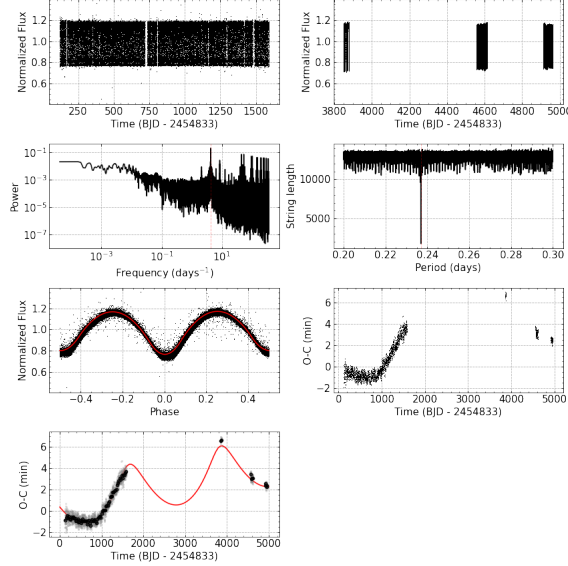


Figure 13. O-C diagram for the binary system KIC 3221207 (TIC 121213501).

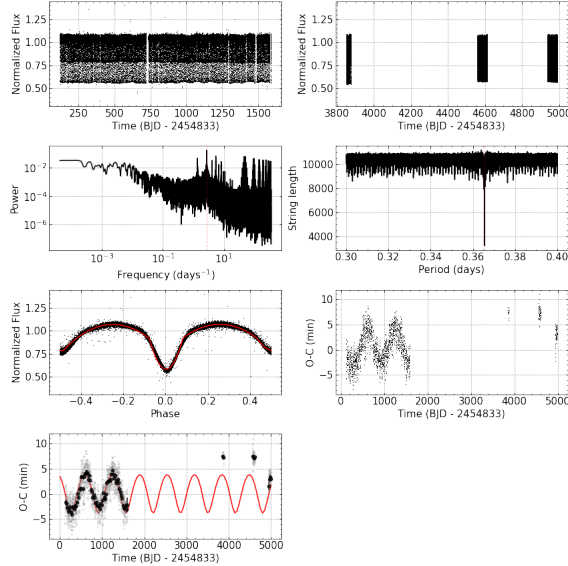


Figure 14. Same analyses of Fig. 11, but for KIC 3228863 (TIC 394179296).

364

A.7. KIC 3936357 (TIC 120499528) Object

365 This object presents a periodic variation in its O-C diagram, Fig. 17, intuiting the presence of a third body around
 366 the binary system with a period $P = 2132.636^{+67.619}_{-47.151}$, in an orbit with eccentricity $e = 0.120^{+0.075}_{-0.061}$, at a distance
 367 $a = 469.656^{+18.435}_{-24.562}$ from its parent stars, with its inclination axis $\omega = 203.482^{+26.213}_{-50.987}$.

368

A.8. KIC 3953981 (TIC 137152301) Object

369 This object presents a periodic variation in its O-C diagram, Fig. 18, intuiting the presence of a third body around
 370 the binary system with a period $P = 2862.477^{+94.503}_{-122.901}$, in an orbit with eccentricity $e = 0.223^{+0.095}_{-0.069}$, at a distance
 371 $a = 220.574^{+19.656}_{-13.916}$ from its parent stars, with its inclination axis $\omega = 254.738^{+28.379}_{-42.287}$.

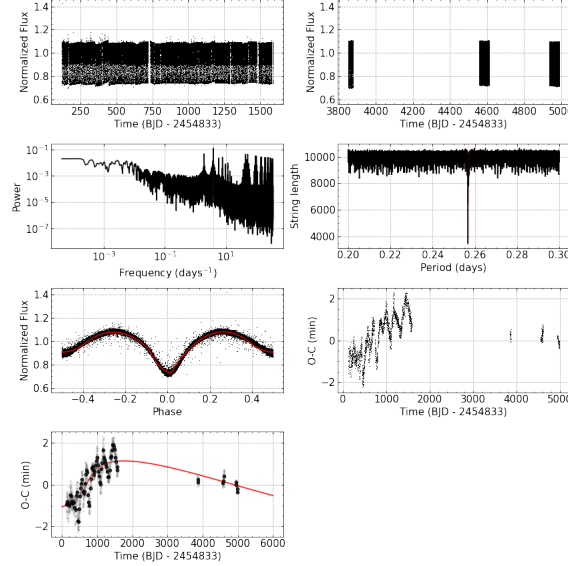


Figure 15. O-C diagram for the binary system KIC 3448245 (TIC 137687487).

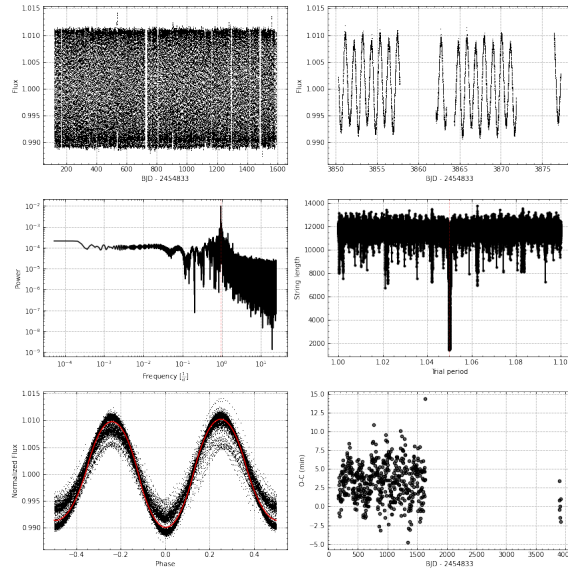


Figure 16. O-C diagram for the binary system KIC 3641446 (TIC 122303843).

A.9. *KIC 4450976, (TIC 121215583) Object*

This object presents a periodic variation in its O-C diagram, Fig. 19, intuiting the presence of a third body around the binary system with a period $P = 2546.115^{+161.201}_{-203.502}$, in an orbit with eccentricity $e = 0.313^{+0.150}_{-0.201}$, at a distance $a = 34367.104^{+2451.117}_{-2702.057}$ from its parent stars, with its inclination axis $\omega = 297.249^{+34.620}_{-33.954}$.

A.10. *KIC 4451148 (TIC 121274442) Object*

This object presents a periodic variation in its O-C diagram, Fig. 20, intuiting the presence of a third body around the binary system with a period $P = 769.411^{+6.770}_{-10.758}$, in an orbit with eccentricity $e = 0.466^{+0.087}_{-0.023}$, at a distance $a = 909.084^{+315.158}_{-185.851}$ from its parent stars, with its inclination axis $\omega = 165.080^{+1.177}_{-7.611}$.

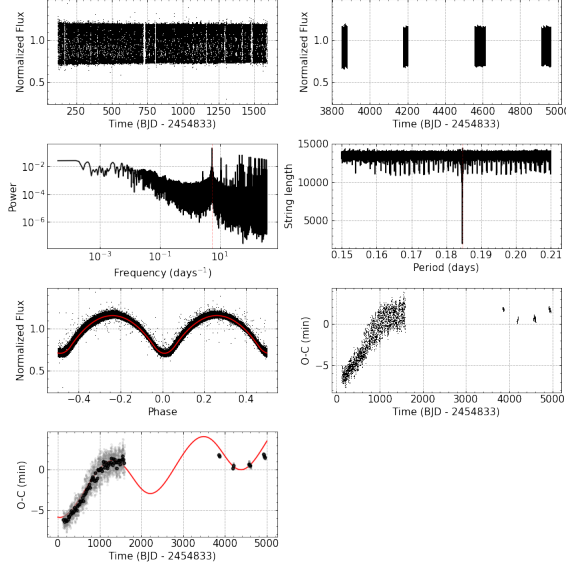


Figure 17. O-C diagram for the binary system KIC 3936357 (TIC 120499528).

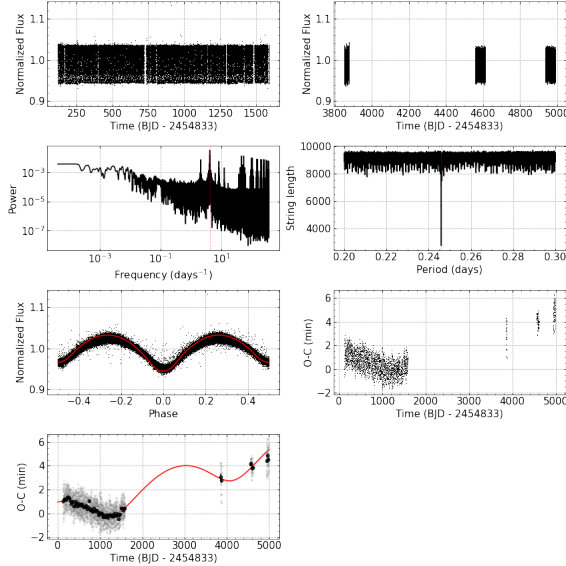


Figure 18. O-C diagram for the binary system KIC 3953981 (TIC 137152301).

A.11. *KIC 4647652 (TIC 122070918) Object*

This object presents a periodic variation in its O-C diagram, Fig. 21, intuiting the presence of a third body around the binary system with a period $P = 755.235^{+19.495}_{-13.418}$, in an orbit with eccentricity $e = 0.245^{+0.290}_{-0.147}$, at a distance $a = 636.222^{+147.225}_{-143.015}$ from its parent stars, with its inclination axis $\omega = 239.394^{+58.689}_{-21.004}$.

A.12. *KIC 4758368 (TIC 138893145) Object*

This object presents a periodic variation in its O-C diagram, Fig. 22, intuiting the presence of a third body around the binary system with a period $P = 2473.632^{+318.289}_{-147.137}$, in an orbit with eccentricity $e = 0.876^{+0.083}_{-0.056}$, at a distance $a = 826.152^{+98.935}_{-99.057}$ from its parent stars, with its inclination axis $\omega = 101.987^{+13.423}_{-12.392}$.

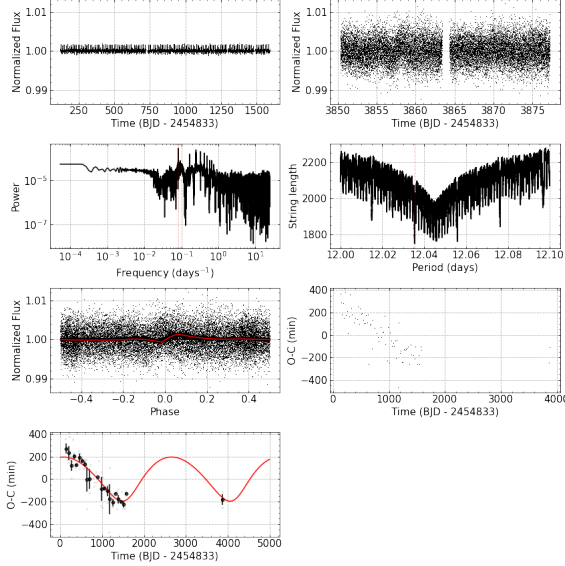


Figure 19. O-C diagram for the binary system KIC 4450976 (TIC 121215583).

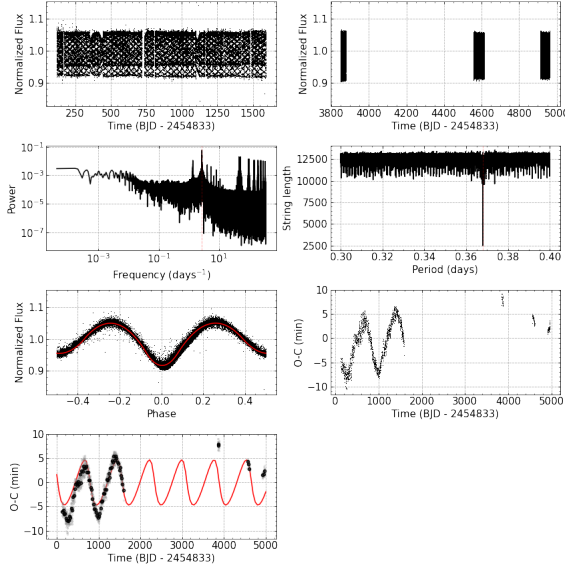


Figure 20. Same analyses of Fig. 11, but for KIC 4451148 (TIC 121274442).

388

A.13. *KIC 4851217 (TIC 184246521) Object*

389 This object presents a periodic variation in its O-C diagram, Fig. 23, intuiting the presence of a third body around
 390 the binary system with a period $P = 2473.632^{+318.289}_{-147.137}$, in an orbit with eccentricity $e = 0.876^{+0.083}_{-0.056}$, at a distance
 391 $a = 826.152^{+98.935}_{-99.057}$ from its parent stars, with its inclination axis $\omega = 101.987^{+13.423}_{-12.392}$.

392

A.14. *KIC 4909422 (TIC 121108244) Object*

393 This object presents a periodic variation in its O-C diagram, Fig. 24, intuiting the presence of a third body around
 394 the binary system with a period $P = 6582.935^{+927.321}_{-1415.082}$, in an orbit with eccentricity $e = 0.839^{+0.131}_{-0.096}$, at a distance
 395 $a = 787.887^{+39.067}_{-99.774}$ from its parent stars, with its inclination axis $\omega = 6.695^{+6.849}_{-4.825}$.

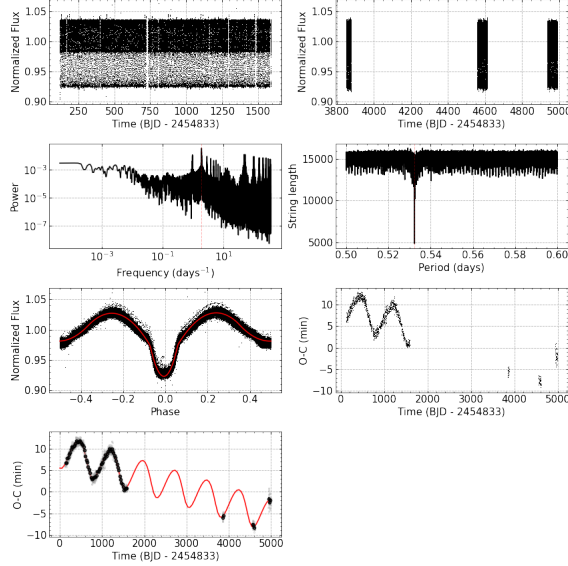


Figure 21. Same analyses of Fig. 11, but for KIC 4647652 (TIC 122070918).

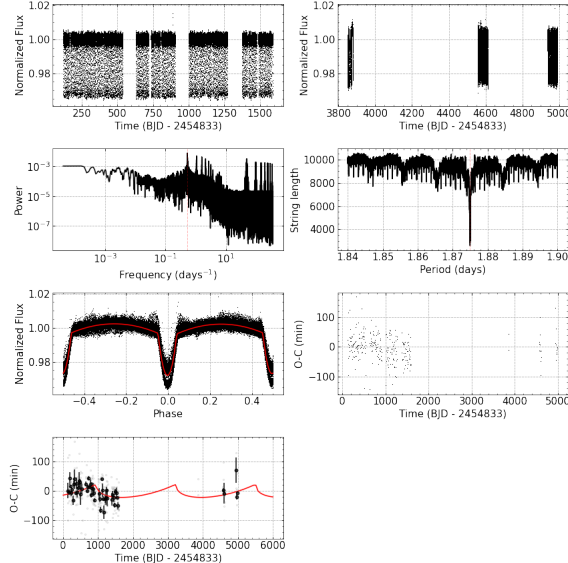


Figure 22. Same analyses of Fig. 22, but for KIC 4758368 (TIC 138893145).

A.15. *KIC 4909707 (TIC 121119758) Object*

This object presents a periodic variation in its O-C diagram, Fig. 25, intuiting the presence of a third body around the binary system with a period $P = 513.727^{+0.617}_{-0.517}$, in an orbit with eccentricity $e = 0.657^{+0.029}_{-0.027}$, at a distance $a = 2066.938^{+71.794}_{-65.971}$ from its parent stars, with its inclination axis $\omega = 358.498^{+1.114}_{-1.642}$ and linear parameters fits at $A = -6.858^{+0.110}_{-0.107}$ and $B = 0.003^{+0.000}_{-0.000}$.

A.16. *KIC 4945588 (TIC 169079394) Object*

This object presents a periodic variation in its O-C diagram, Fig. 26, intuiting the presence of a third body around the binary system with a period $P = 1607.893^{+29.331}_{-140.789}$, in an orbit with eccentricity $e = 0.871^{+0.046}_{-0.045}$, at a distance $a = 1289.577^{+32.368}_{-66.834}$ from its parent stars, with its inclination axis $\omega = 134.791^{+5.397}_{-6.424}$.

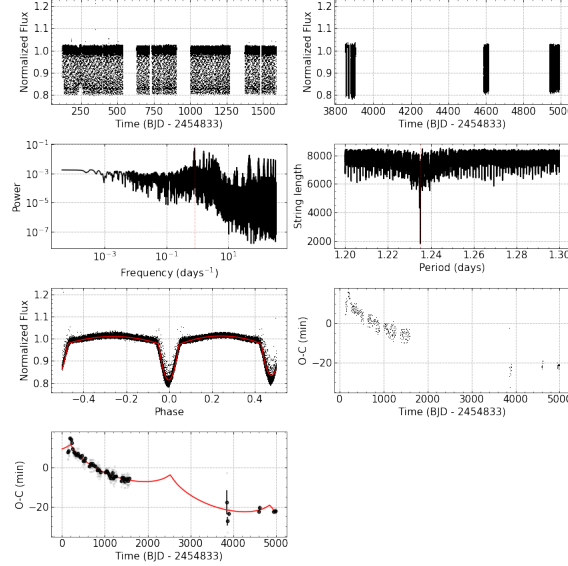


Figure 23. O-C diagram for the binary system KIC 4851217 (TIC 184246521).

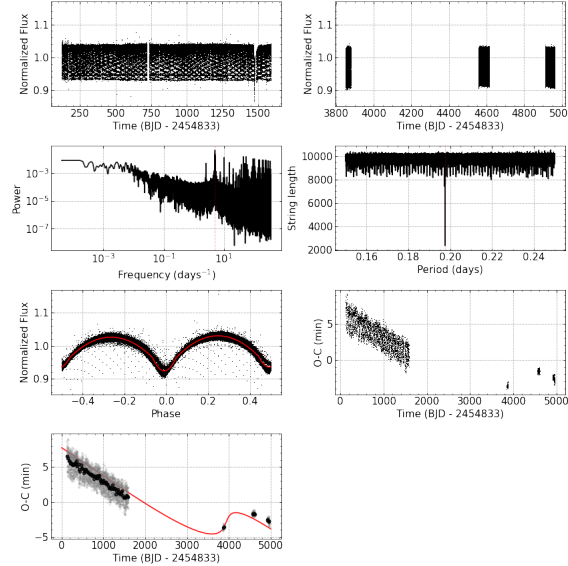


Figure 24. O-C diagram for the binary system KIC 4909422 (TIC 121108244).

A.17. *KIC 4999260 (TIC 121460104) Object*

405 This object presents a periodic variation in its O-C diagram, Fig. 27, intuiting the presence of a third body around
 406 the binary system with a period $P = 41607.891^{+1184.572}_{-1247.838}$, in an orbit with eccentricity $e = 0.895^{+0.027}_{-0.021}$, at a distance
 407 $a = 1276.685^{+75.891}_{-50.225}$ from its parent stars, with its inclination axis $\omega = 226.484^{+4.791}_{-9.178}$.

A.18. *KIC 5022573 (TIC 138960108) Object*

409 This object presents a periodic variation in its O-C diagram, Fig. 28, intuiting the presence of a third body around
 410 the binary system with a period $P = 1826.598^{+113.755}_{-133.477}$, in an orbit with eccentricity $e = 0.766^{+0.083}_{-0.061}$, at a distance
 411 $a = 2900.240^{+275.154}_{-298.752}$ from its parent stars, with its inclination axis $\omega = 26.089^{+12.937}_{-10.238}$.

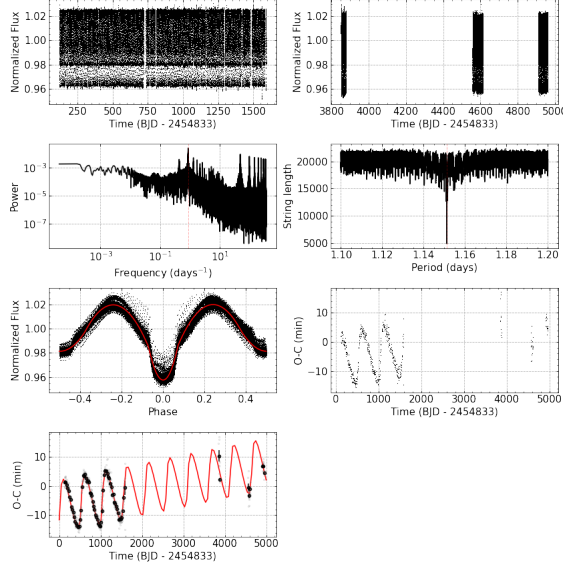


Figure 25. Same analyses of Fig. 11, but for KIC 4909707 (TIC 121119758).

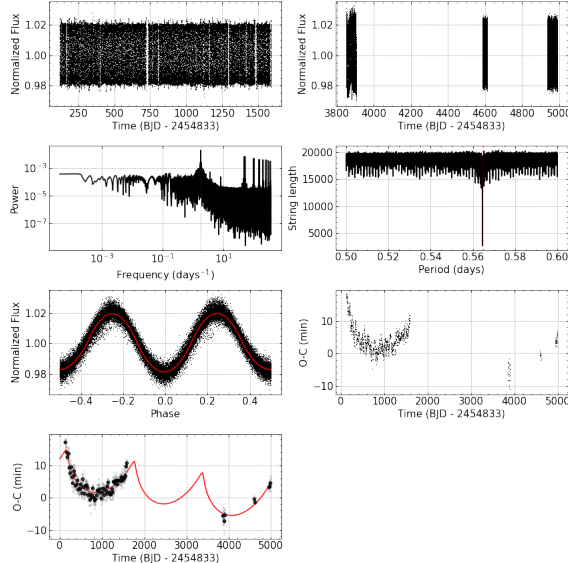


Figure 26. O-C diagram for the binary system KIC 4945588 (TIC 169079394).

A.19. *KIC 5264818 (TIC 121732964) Object*

This object presents a periodic variation in its O-C diagram, Fig. 29, intuiting the presence of a third body around the binary system with a period $P = 282.272^{+2.898}_{-4.298}$, in an orbit with eccentricity $e = 0.436^{+0.208}_{-0.309}$, at a distance $a = 486.055^{+59.249}_{-177.430}$ from its parent stars, with its inclination axis $\omega = 342.066^{+13.325}_{-45.838}$ and linear parameters fits at $A = 3.680^{+0.351}_{-0.301}$ and $B = -0.000^{+0.000}_{-0.000}$.

A.20. *KIC 5296877 (TIC 169181296) Object*

This object presents a periodic variation in its O-C diagram, Fig. 30, intuiting the presence of a third body around the binary system with a period $P = 4962.088^{+11.012}_{-16.105}$, in an orbit with eccentricity $e = 0.728^{+0.010}_{-0.007}$, at a distance $a = 929.247^{+4.982}_{-6.414}$ from its parent stars, with its inclination axis $\omega = 87.015^{+0.658}_{-0.689}$.

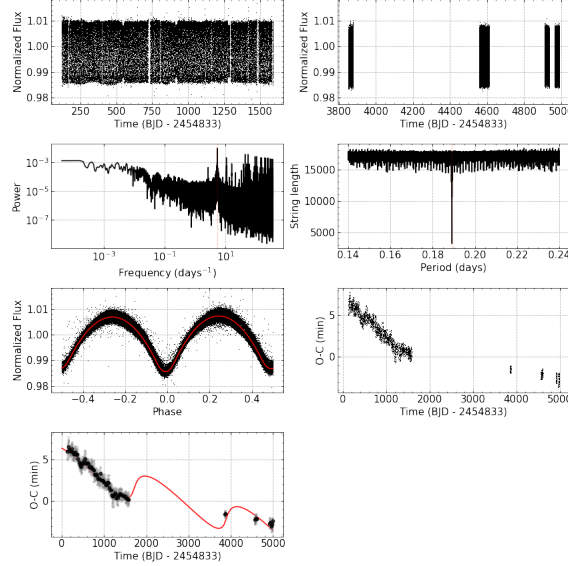


Figure 27. O-C diagram for the binary system KIC 4999260 (TIC 121460104).

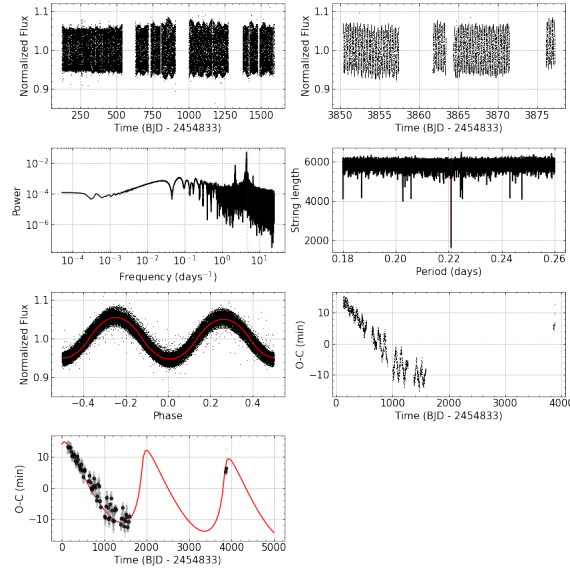


Figure 28. O-C diagram for the binary system KIC 5022573 (TIC 138960108).

A.21. *KIC 5513861 (TIC 120251815) Object*

This object presents a periodic variation in its O-C diagram, Fig. 31, intuiting the presence of a third body around the binary system with a period $P = 2113.335^{+5.927}_{-6.342}$, in an orbit with eccentricity $e = 0.315^{+0.019}_{-0.029}$, at a distance $a = 3763.359^{+90.637}_{-88.600}$ from its parent stars, with its inclination axis $\omega = 291.346^{+5.326}_{-5.698}$.

A.22. *KIC 5975712 (TIC 184253728) Object*

This object presents a periodic variation in its O-C diagram, Fig. 32, intuiting the presence of a third body around the binary system with a period $P = 1694.694^{+1.650}_{-2.058}$, in an orbit with eccentricity $e = 0.218^{+0.001}_{-0.000}$, at a distance $a = 1717.176^{+2.114}_{-2.202}$ from its parent stars, with its inclination axis $\omega = 262.443^{+0.358}_{-0.235}$.

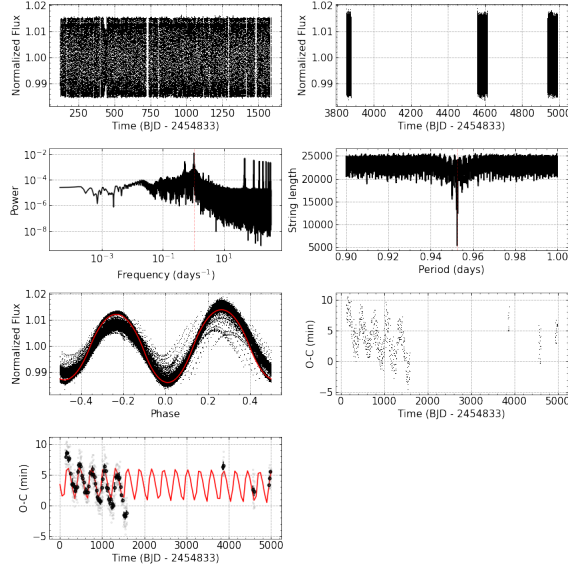


Figure 29. Same analyses of Fig. 11, but for KIC 5264818 (TIC 121732964).

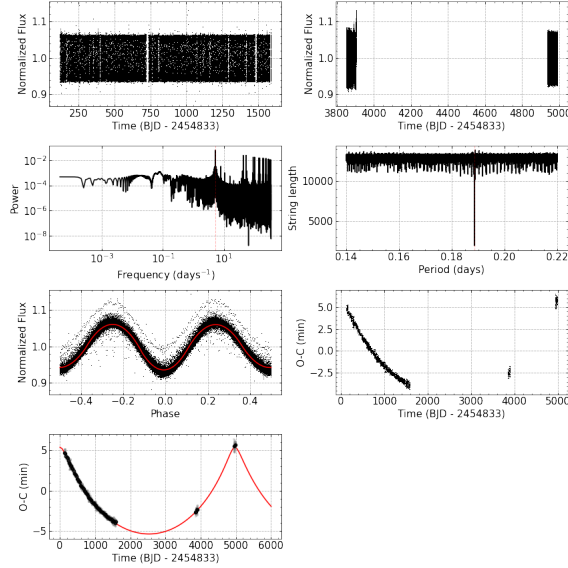


Figure 30. O-C diagram for the binary system KIC 5296877 (TIC 169181296).

A.23. KIC 6187893 (TIC 120576722) Object

430 This object presents a periodic variation in its O-C diagram, Fig. 33, intuiting the presence of a third body around
 431 the binary system with a period $P = 2028.925^{+5.819}_{-5.788}$, in an orbit with eccentricity $e = 0.969^{+0.004}_{-0.006}$, at a distance
 432 $a = 15566.140^{+1116.612}_{-1159.858}$ from its parent stars, with its inclination axis $\omega = 354.398^{+0.646}_{-0.703}$.

A.24. KIC 6205460 (TIC 137408317) Object

434 This object presents a periodic variation in its O-C diagram, Fig. 34, intuiting the presence of a third body around
 435 the binary system with a period $P = 2311.862^{+83.952}_{-29.020}$, in an orbit with eccentricity $e = 0.426^{+0.019}_{-0.071}$, at a distance
 436 $a = 37561.143^{+214.540}_{-973.443}$ from its parent stars, with its inclination axis $\omega = 233.491^{+4.345}_{-1.748}$.

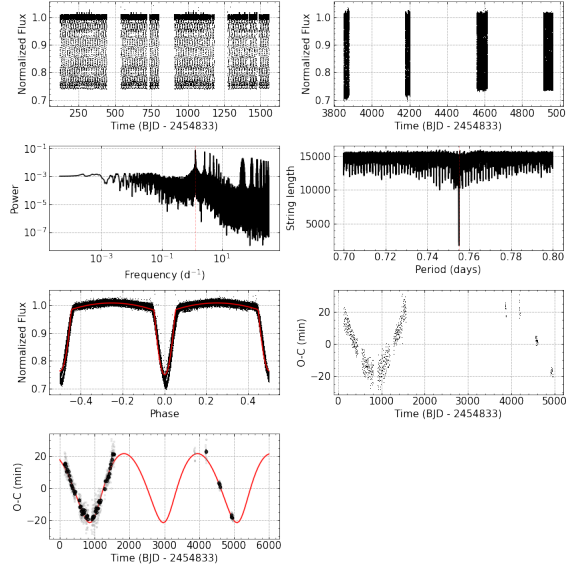


Figure 31. O-C diagram for the binary system KIC 5513861 (TIC 120251815).

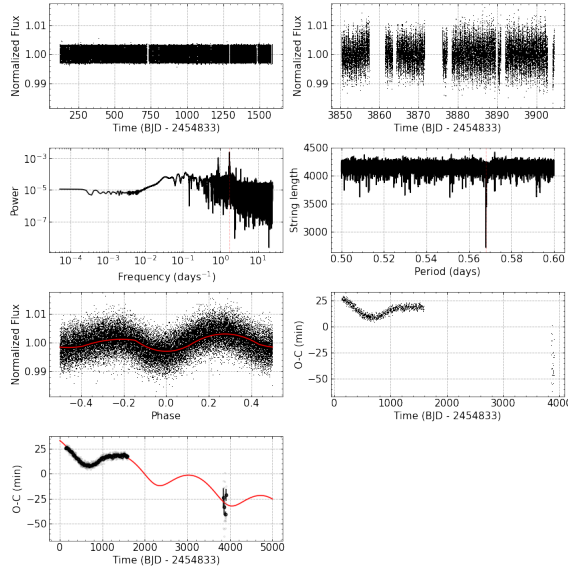


Figure 32. O-C diagram for the binary system KIC 5975712 (TIC 184253728).

A.25. *KIC 6353203 (TIC 121463130) Object*

438 This object presents a periodic variation in its O-C diagram, Fig. 35, intuiting the presence of a third body around
 439 the binary system with a period $P = 2449.628^{+19.370}_{-7.118}$, in an orbit with eccentricity $e = 0.575^{+0.057}_{-0.069}$, at a distance
 440 $a = 2535.311^{+140.257}_{-264.969}$ from its parent stars, with its inclination axis $\omega = 33.826^{+9.897}_{-2.290}$.

A.26. *KIC 6462057 (TIC 169175441) Object*

442 This object presents a periodic variation in its O-C diagram, Fig. 36, intuiting the presence of a third body around
 443 the binary system with a period $P = 4926.320^{+359.711}_{-147.307}$, in an orbit with eccentricity $e = 0.637^{+0.080}_{-0.177}$, at a distance
 444 $a = 410.767^{+31.402}_{-42.634}$ from its parent stars, with its inclination axis $\omega = 76.324^{+18.082}_{-11.176}$.

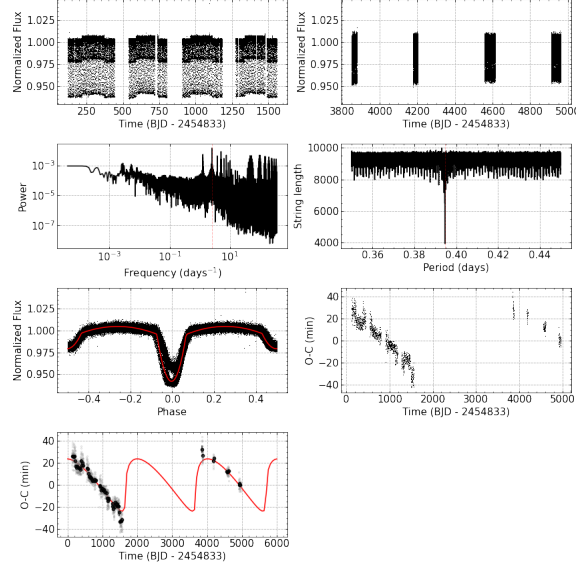


Figure 33. O-C diagram for the binary system KIC 6187893 (TIC 120576722).

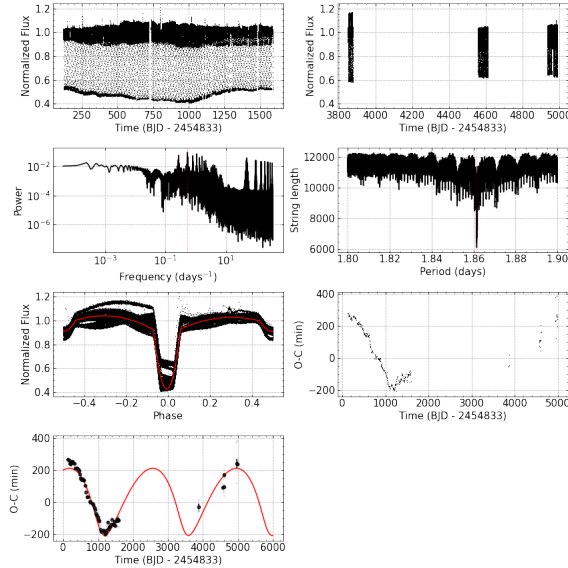


Figure 34. O-C diagram for the binary system KIC 6205460 (TIC 137408317).

A.27. KIC 7259917 (TIC 164463075) Object

This object presents a periodic variation in its O-C diagram, Fig. 37, intuiting the presence of a third body around the binary system with a period $P = 4729.394^{+441.635}_{-196.787}$, in an orbit with eccentricity $e = 0.720^{+0.063}_{-0.222}$, at a distance $a = 794.232^{+124.608}_{-171.657}$ from its parent stars, with its inclination axis $\omega = 223.241^{+21.873}_{-16.910}$.

A.28. KIC 7375612 (TIC 271671189) Object

This object presents a periodic variation in its O-C diagram, Fig. 38, intuiting the presence of a third body around the binary system with a period $P = 2123.456^{+15.279}_{-7.569}$, in an orbit with eccentricity $e = 0.098^{+0.074}_{-0.028}$, at a distance $a = 1221.564^{+45.153}_{-18.592}$ from its parent stars, with its inclination axis $\omega = 302.775^{+39.354}_{-19.329}$.

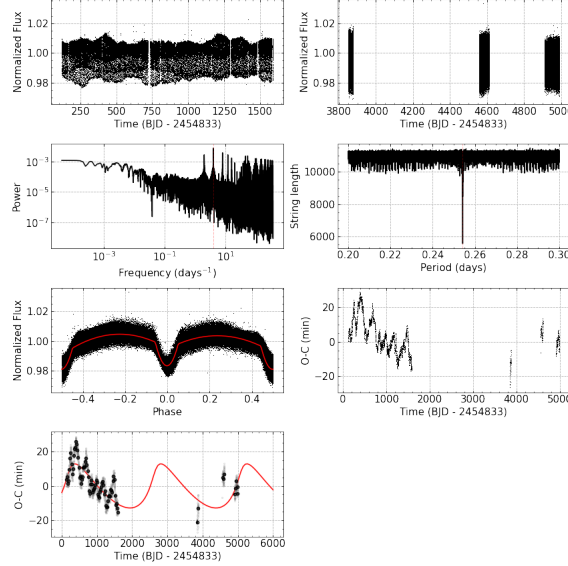


Figure 35. O-C diagram for the binary system KIC 6353203 (TIC 121463130).

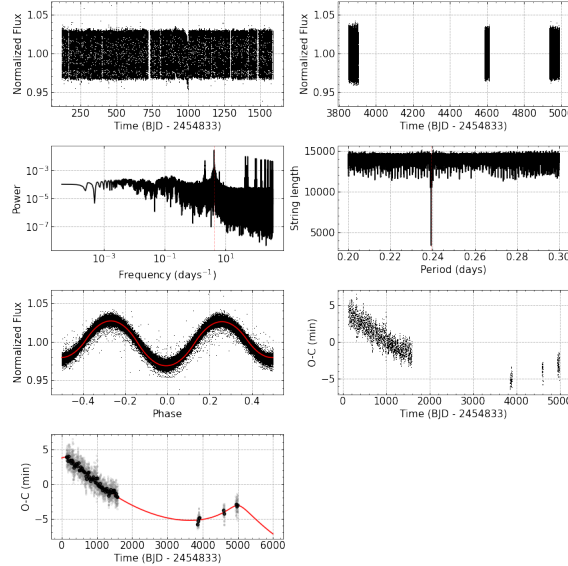


Figure 36. O-C diagram for the binary system KIC 6462057 (TIC 169175441).

A.29. *KIC 7385478 (TIC 273501820) Object*

454 This object presents a periodic variation in its O-C diagram, Fig. 39, intuiting the presence of a third body around
 455 the binary system with a period $P = 1360.065^{+76.397}_{-101.476}$, in an orbit with eccentricity $e = 0.782^{+0.148}_{-0.363}$, at a distance
 456 $a = 2892.213^{+287.804}_{-627.328}$ from its parent stars, with its inclination axis $\omega = 59.734^{+24.105}_{-25.564}$.

A.30. *KIC 7431703 (TIC 158431889) Object*

458 This object presents a periodic variation in its O-C diagram, Fig. 40, intuiting the presence of a third body around
 459 the binary system with a period $P = 1820.383^{+42.684}_{-105.177}$, in an orbit with eccentricity $e = 0.448^{+0.121}_{-0.158}$, at a distance
 460 $a = 193.698^{+45.269}_{-23.174}$ from its parent stars, with its inclination axis $\omega = 133.419^{+48.678}_{-38.020}$.

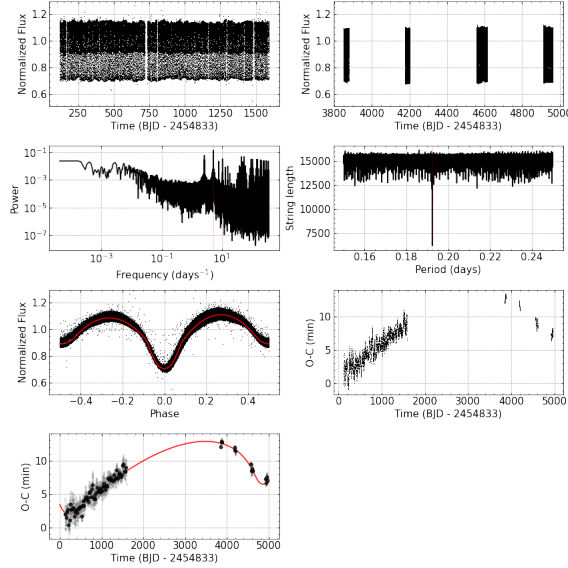


Figure 37. O-C diagram for the binary system KIC 7259917 (TIC 164463075).

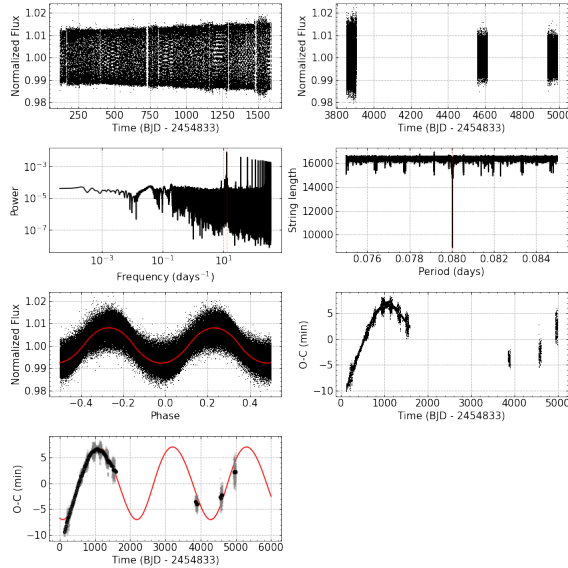


Figure 38. O-C diagram for the binary system KIC 7375612 (TIC 271671189).

A.31. KIC 7440742 (TIC 159444225) Object

This object presents a periodic variation in its O-C diagram, Fig. 41, intuiting the presence of a third body around the binary system with a period $P = 2003.253^{+133.920}_{-126.183}$, in an orbit with eccentricity $e = 0.983^{+0.005}_{-0.013}$, at a distance $a = 3175.282^{+129.578}_{-270.423}$ from its parent stars, with its inclination axis $\omega = 11.419^{+1.766}_{-3.858}$.

A.32. KIC 7457163 (TIC 271539287) Object

This object presents a periodic variation in its O-C diagram, Fig. 42, intuiting the presence of a third body around the binary system with a period $P = 6255.520^{+135.002}_{-193.789}$, in an orbit with eccentricity $e = 0.527^{+0.062}_{-0.039}$, at a distance $a = 2751.917^{+61.453}_{-41.633}$ from its parent stars, with its inclination axis $\omega = 278.115^{+8.270}_{-3.766}$.

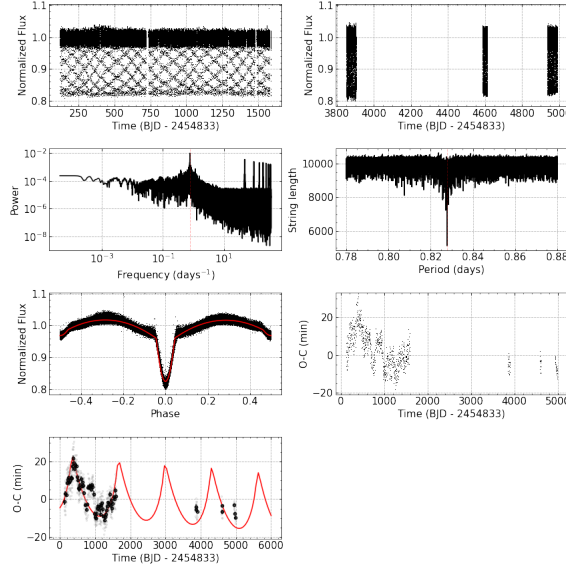


Figure 39. O-C diagram for the binary system KIC 7385478 (TIC 273501820).

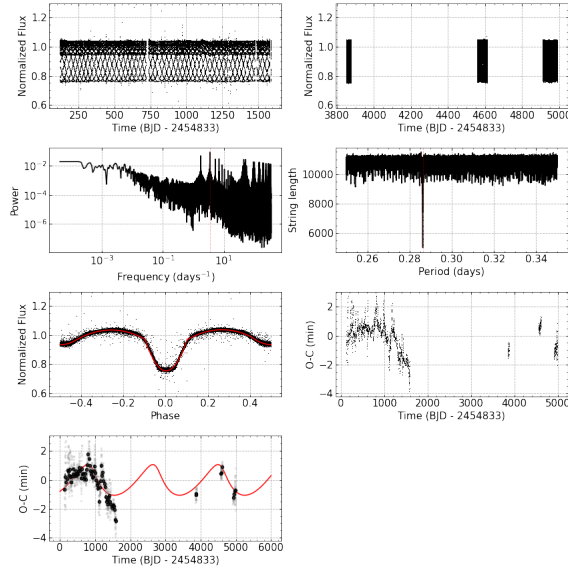


Figure 40. O-C diagram for the binary system KIC 7431703 (TIC 158431889).

A.33. *KIC 7512381 (TIC 158218818) Object*

470 This object presents a periodic variation in its O-C diagram, Fig. 43, intuiting the presence of a third body around
 471 the binary system with a period $P = 6805.413^{+249.021}_{-135.070}$, in an orbit with eccentricity $e = 0.411^{+0.040}_{-0.131}$, at a distance
 472 $a = 1298.333^{+127.638}_{-41.743}$ from its parent stars, with its inclination axis $\omega = 340.888^{+7.394}_{-5.227}$.

A.34. *KIC 7690843 (TIC 271158877) Object*

474 This object presents a periodic variation in its O-C diagram, Fig. 44, intuiting the presence of a third body around
 475 the binary system with a period $P = 2714.623^{+60.236}_{-72.170}$, in an orbit with eccentricity $e = 0.752^{+0.058}_{-0.152}$, at a distance
 476 $a = 2435.466^{+384.915}_{-494.907}$ from its parent stars, with its inclination axis $\omega = 340.293^{+7.820}_{-10.974}$.

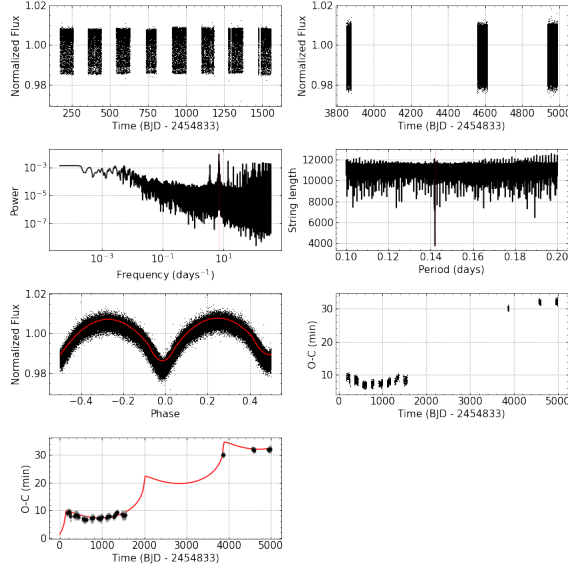


Figure 41. O-C diagram for the binary system KIC 7440742 (TIC 159444225).

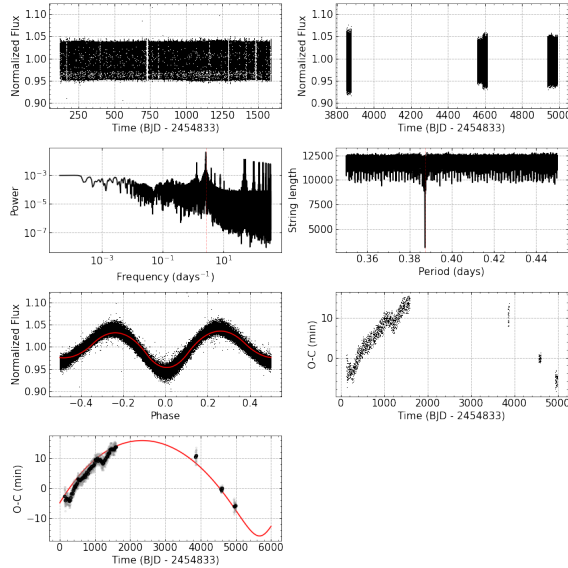


Figure 42. O-C diagram for the binary system KIC 7457163 (TIC 271539287).

A.35. KIC 7765894 (TIC 271967202) Object

478 This object presents a periodic variation in its O-C diagram, Fig. 45, intuiting the presence of a third body around
 479 the binary system with a period $P = 463.815^{+3.584}_{-5.356}$, in an orbit with eccentricity $e = 0.270^{+0.073}_{-0.088}$, at a distance
 480 $a = 3831.739^{+874.241}_{-406.815}$ from its parent stars, with its inclination axis $\omega = 142.982^{+33.786}_{-16.853}$.

A.36. KIC 7766185 (TIC 272176884) Object

482 This object presents a periodic variation in its O-C diagram, Fig. 46, intuiting the presence of a third body around
 483 the binary system with a period $P = 1860.287^{+99.837}_{-87.249}$, in an orbit with eccentricity $e = 0.945^{+0.015}_{-0.024}$, at a distance
 484 $a = 88.601^{+10.424}_{-12.943}$ from its parent stars, with its inclination axis $\omega = 353.253^{+5.047}_{-9.173}$.

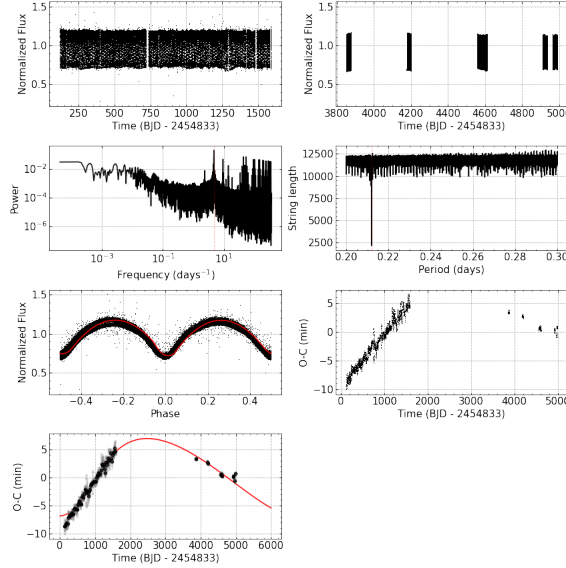


Figure 43. O-C diagram for the binary system KIC 7512381 (TIC 158218818).

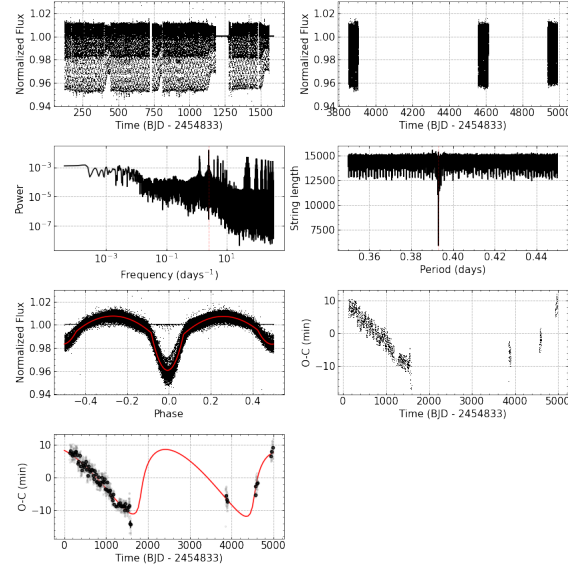


Figure 44. O-C diagram for the binary system KIC 7690843 (TIC 271158877).

A.37. KIC 7816201 (TIC 159105713) Object

486 This object presents a periodic variation in its O-C diagram, Fig. 47, intuiting the presence of a third body around
 487 the binary system with a period $P = 2328.001^{+209.934}_{-397.908}$, in an orbit with eccentricity $e = 0.696^{+0.074}_{-0.124}$, at a distance
 488 $a = 320.107^{+17.816}_{-22.707}$ from its parent stars, with its inclination axis $\omega = 61.045^{+35.826}_{-26.856}$.

A.38. KIC 7938870 (TIC 123416563) Object

491 This object presents a periodic variation in its O-C diagram, Fig. 48, intuiting the presence of a third body around
 492 the binary system with a period $P = 2100.595^{+31.818}_{-32.686}$, in an orbit with eccentricity $e = 0.627^{+0.094}_{-0.022}$, at a distance
 493 $a = 486.852^{+41.826}_{-14.625}$ from its parent stars, with its inclination axis $\omega = 302.126^{+8.472}_{-6.225}$.

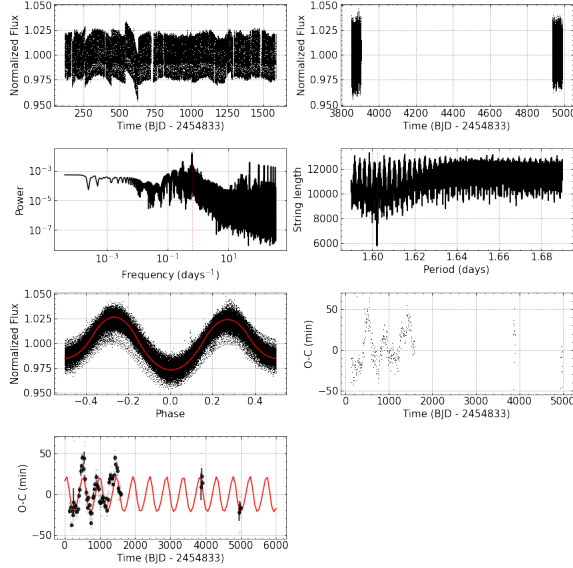


Figure 45. Same analyses of Fig. 11, but for KIC 7765894 (TIC 271967202).

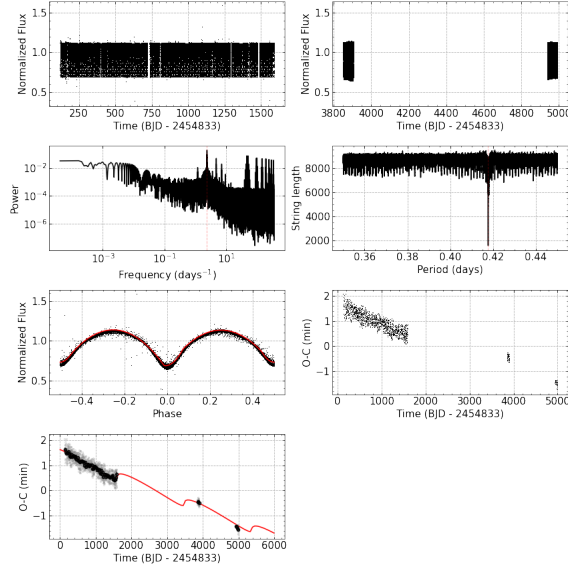


Figure 46. O-C diagram for the binary system KIC 7766185 (TIC 272176884).

A.39. *KIC 7950962 (TIC 158726046) Object*

This object presents a periodic variation in its O-C diagram, Fig. 49, intuiting the presence of a third body around the binary system with a period $P = 3085.157^{+100.353}_{-116.633}$, in an orbit with eccentricity $e = 0.075^{+0.053}_{-0.055}$, at a distance $a = 309.409^{+18.086}_{-30.892}$ from its parent stars, with its inclination axis $\omega = 172.259^{+3.845}_{-5.776}$.

A.40. *KIC 8043961 (TIC 272609309) Object*

This object presents a periodic variation in its O-C diagram, Fig. 50, intuiting the presence of a third body around the binary system with a period $P = 422.710^{+1.645}_{-1.526}$, in an orbit with eccentricity $e = 0.399^{+0.185}_{-0.121}$, at a distance $a = 585.481^{+74.753}_{-59.217}$ from its parent stars, with its inclination axis $\omega = 232.003^{+21.284}_{-26.824}$.

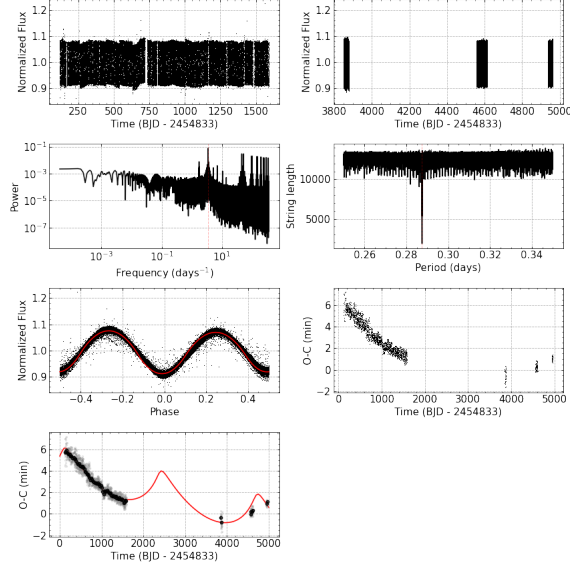


Figure 47. O-C diagram for the binary system KIC 7816201 (TIC 159105713).

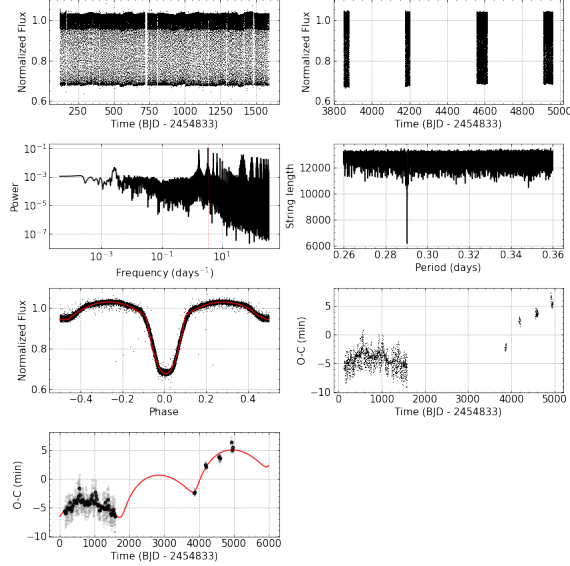


Figure 48. O-C diagram for the binary system KIC 7938870 (TIC 123416563).

A.41. *KIC 8045121 (TIC 272941454) Object*

502 This object presents a periodic variation in its O-C diagram, Fig. 51, intuiting the presence of a third body around
 503 the binary system with a period $P = 890.971^{+14.033}_{-17.999}$, in an orbit with eccentricity $e = 0.349^{+0.085}_{-0.122}$, at a distance
 504 $a = 856.664^{+130.413}_{-86.810}$ from its parent stars, with its inclination axis $\omega = 178.152^{+31.503}_{-31.898}$ and linear parameters fits at
 505 $A = 0.755^{+0.138}_{-0.066}$ and $B = 0.003^{+0.001}_{-0.001}$.

A.42. *KIC 8189196 (TIC 268302473) Object*

506 This object presents a periodic variation in its O-C diagram, Fig. 52, intuiting the presence of a third body around
 507 the binary system with a period $P = 3903.002^{+24.689}_{-30.695}$, in an orbit with eccentricity $e = 0.980^{+0.003}_{-0.004}$, at a distance
 508 $a = 12579.602^{+931.164}_{-840.971}$ from its parent stars, with its inclination axis $\omega = 352.082^{+0.671}_{-0.857}$.

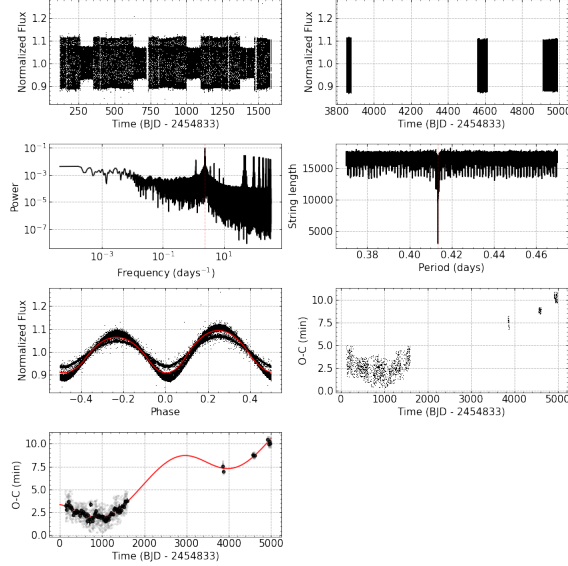


Figure 49. O-C diagram for the binary system KIC 7950962 (TIC 158726046).

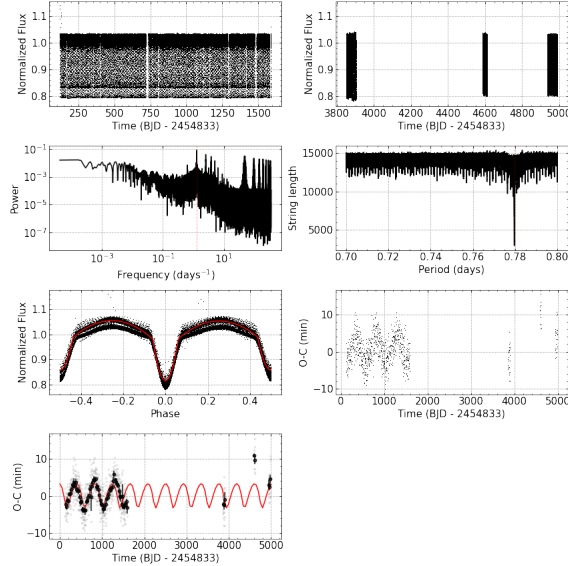


Figure 50. Same analyses of Fig. 11, but for KIC 8043961 (TIC 272609309).

A.43. KIC 8231231 (TIC 159578658) Object

This object presents a periodic variation in its O-C diagram, Fig. 53, intuiting the presence of a third body around the binary system with a period $P = 1909.021^{+50.390}_{-54.438}$, in an orbit with eccentricity $e = 0.949^{+0.021}_{-0.033}$, at a distance $a = 2930.266^{+110.526}_{-401.530}$ from its parent stars, with its inclination axis $\omega = 17.464^{+4.268}_{-4.281}$.

A.44. KIC 8285349 (TIC 352012002) Object

This object presents a periodic variation in its O-C diagram, Fig. 54, intuiting the presence of a third body around the binary system with a period $P = 2042.641^{+16.160}_{-55.476}$, in an orbit with eccentricity $e = 0.522^{+0.022}_{-0.218}$, at a distance $a = 1553.753^{+36.747}_{-102.809}$ from its parent stars, with its inclination axis $\omega = 0.246^{+0.658}_{-0.195}$.

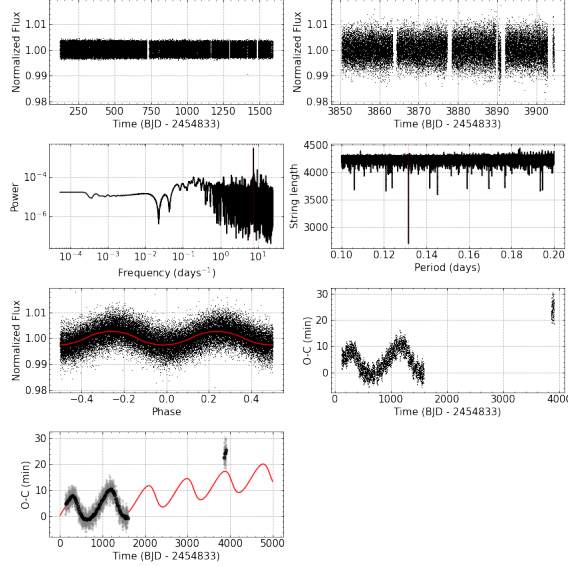


Figure 51. Same analyses of Fig. 11, but for KIC 8045121 (TIC 272941454).

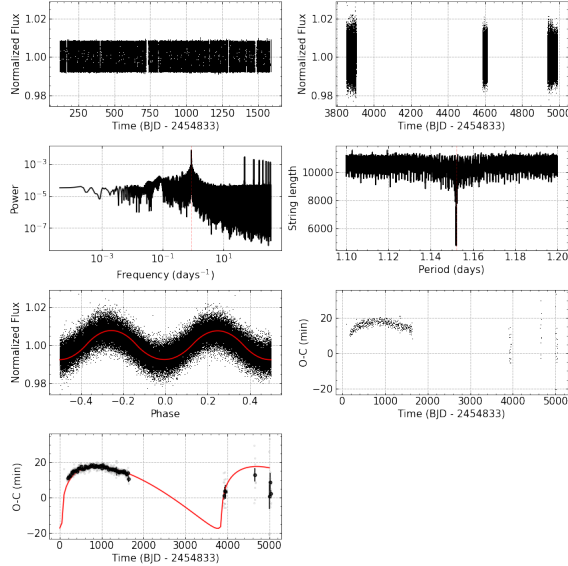


Figure 52. O-C diagram for the binary system KIC 8189196 (TIC 268302473).

519

A.45. KIC 8386865 (TIC 274024023) Object

520 This object presents a periodic variation in its O-C diagram, Fig. 55, intuiting the presence of a third body around
 521 the binary system with a period $P = 294.267^{+0.998}_{-0.874}$, in an orbit with eccentricity $e = 0.421^{+0.055}_{-0.033}$, at a distance
 522 $a = 543.508^{+17.373}_{-19.167}$ from its parent stars, with its inclination axis $\omega = 141.070^{+7.028}_{-6.075}$.

523

A.46. KIC 8397460 (TIC 185286922) Object

524 This object presents a periodic variation in its O-C diagram, Fig. 56, intuiting the presence of a third body around
 525 the binary system with a period $P = 8112.505^{+509.919}_{-443.186}$, in an orbit with eccentricity $e = 0.966^{+0.003}_{-0.003}$, at a distance
 526 $a = 17859.920^{+1277.042}_{-1093.353}$ from its parent stars, with its inclination axis $\omega = 184.634^{+3.200}_{-3.526}$.

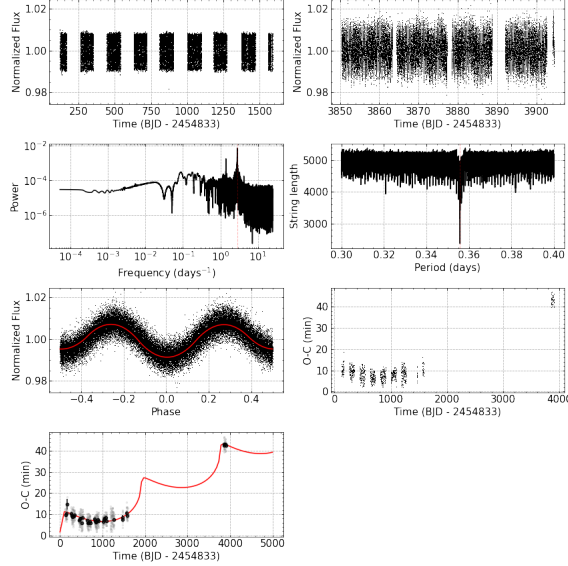


Figure 53. O-C diagram for the binary system KIC 8231231 (TIC 159578658).

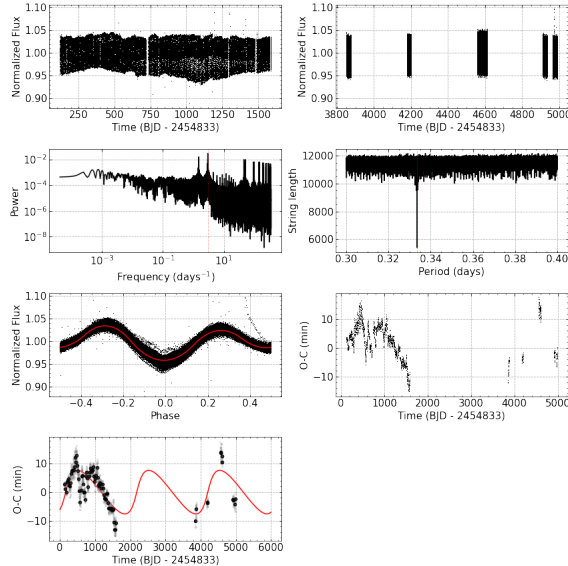


Figure 54. O-C diagram for the binary system KIC 8285349 (TIC 352012002).

A.47. KIC 8579707 (TIC 273865522) Object

This object presents a periodic variation in its O-C diagram, Fig. 57, intuiting the presence of a third body around the binary system with a period $P = 1944.760^{+203.672}_{-24.784}$, in an orbit with eccentricity $e = 0.523^{+0.090}_{-0.037}$, at a distance $a = 767.345^{+60.336}_{-22.646}$ from its parent stars, with its inclination axis $\omega = 274.445^{+12.220}_{-27.352}$.

A.48. KIC 8587792 (TIC 239290086) Object

This object presents a periodic variation in its O-C diagram, Fig. 58, intuiting the presence of a third body around the binary system with a period $P = 5493.004^{+294.492}_{-278.158}$, in an orbit with eccentricity $e = 0.380^{+0.046}_{-0.040}$, at a distance $a = 1206.681^{+74.433}_{-72.220}$ from its parent stars, with its inclination axis $\omega = 320.376^{+8.325}_{-6.775}$.

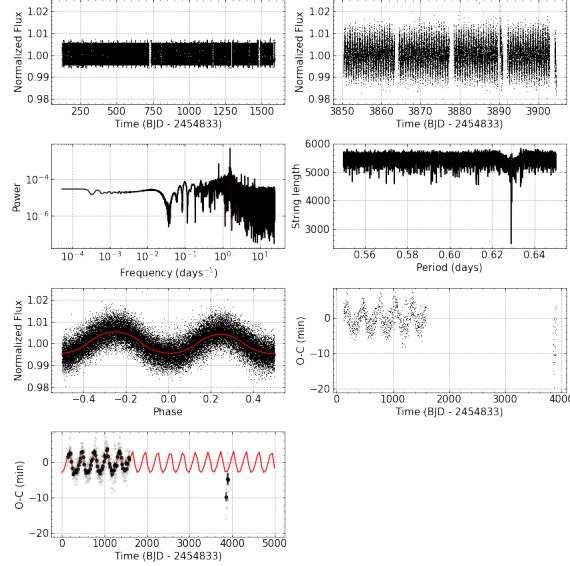


Figure 55. Same analyses of Fig. 11, but for KIC 8386865 (TIC 274024023).

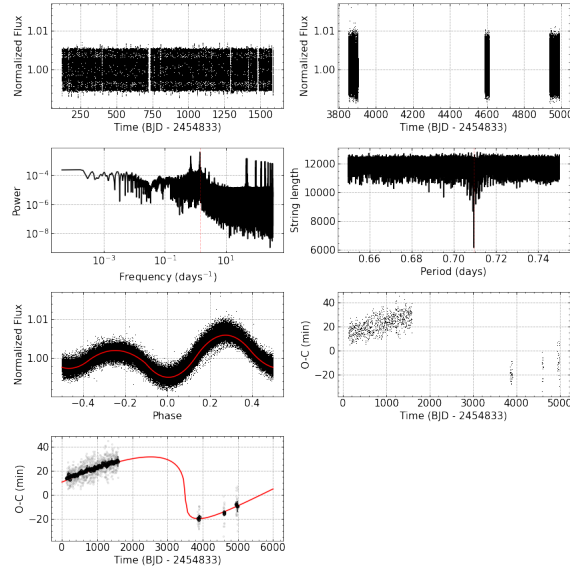


Figure 56. O-C diagram for the binary system KIC 8397460 (TIC 185286922).

535

A.49. *KIC 8758161 (TIC 270615728) Object*

536 This object presents a periodic variation in its O-C diagram, Fig. 59, intuiting the presence of a third body around
 537 the binary system with a period $P = 18453.026^{+3264.951}_{-3355.454}$, in an orbit with eccentricity $e = 0.908^{+0.047}_{-0.069}$, at a distance
 538 $a = 8615.186^{+1034.901}_{-1451.131}$ from its parent stars, with its inclination axis $\omega = 8.511^{+9.509}_{-4.650}$.

539

A.50. *KIC 8894630 (TIC 271352011) Object*

540 This object presents a periodic variation in its O-C diagram, Fig. 60, intuiting the presence of a third body around
 541 the binary system with a period $P = 7635.890^{+351.320}_{-315.610}$, in an orbit with eccentricity $e = 0.737^{+0.043}_{-0.030}$, at a distance
 542 $a = 5539.682^{+502.895}_{-297.206}$ from its parent stars, with its inclination axis $\omega = 14.359^{+4.427}_{-4.471}$.

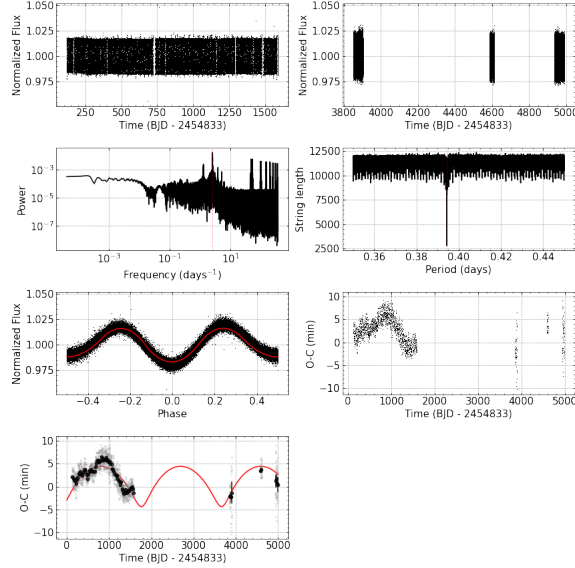


Figure 57. O-C diagram for the binary system KIC 8579707 (TIC 273865522).

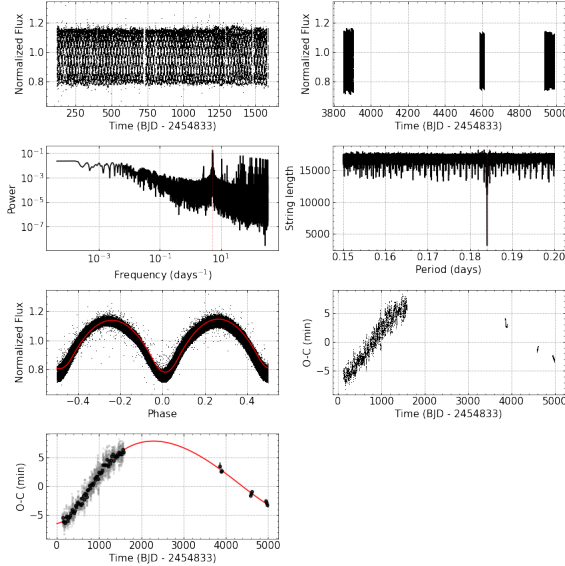


Figure 58. O-C diagram for the binary system KIC 8587792 (TIC 239290086).

543

A.51. *KIC 9083523 (TIC 159169838) Object*

544 This object presents a periodic variation in its O-C diagram, Fig. 61, intuiting the presence of a third body around
 545 the binary system with a period $P = 2200.587^{+36.070}_{-16.377}$, in an orbit with eccentricity $e = 0.370^{+0.084}_{-0.090}$, at a distance
 546 $a = 621.439^{+29.266}_{-30.823}$ from its parent stars, with its inclination axis $\omega = 202.850^{+10.495}_{-7.422}$.

547

A.52. *KIC 9181877 (TIC 239309691) Object*

548 This object presents a periodic variation in its O-C diagram, Fig. 62, intuiting the presence of a third body around
 549 the binary system with a period $P = 1830.374^{+20.089}_{-49.420}$, in an orbit with eccentricity $e = 0.596^{+0.054}_{-0.051}$, at a distance
 550 $a = 2570.357^{+286.471}_{-143.622}$ from its parent stars, with its inclination axis $\omega = 44.869^{+9.228}_{-9.783}$.

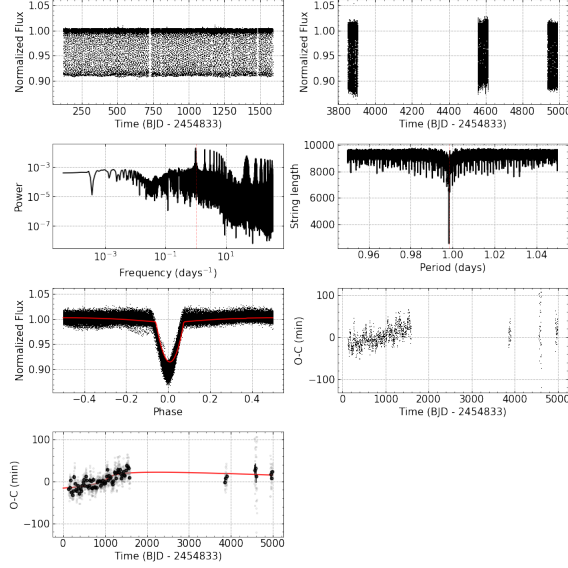


Figure 59. O-C diagram for the binary system KIC 8758161 (TIC 270615728).

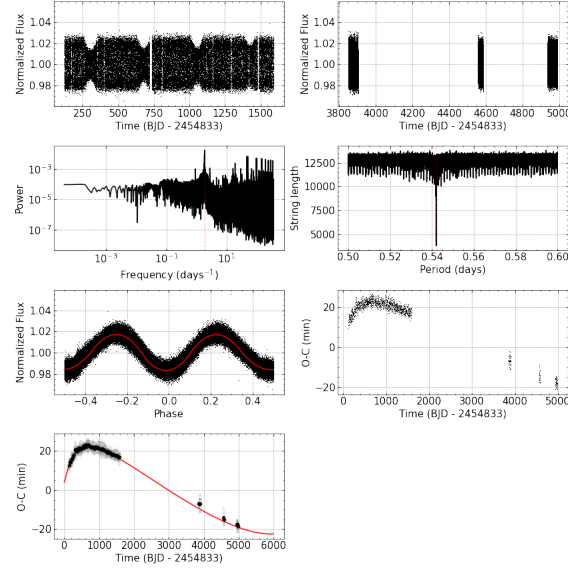


Figure 60. O-C diagram for the binary system KIC 8894630 (TIC 271352011).

551

A.53. *KIC 9345838 (TIC 275575030) Object*

552 This object presents a periodic variation in its O-C diagram, Fig. 63, intuiting the presence of a third body around
 553 the binary system with a period $P = 2497.096^{+5.248}_{-7.119}$, in an orbit with eccentricity $e = 0.969^{+0.013}_{-0.009}$, at a distance
 554 $a = 3366.064^{+932.765}_{-754.234}$ from its parent stars, with its inclination axis $\omega = 6.993^{+0.821}_{-1.239}$.

555

A.54. *KIC 9365025 (TIC 268711288) Object*

556 This object presents a periodic variation in its O-C diagram, Fig. 64, intuiting the presence of a third body around
 557 the binary system with a period $P = 731.626^{+3.616}_{-2.190}$, in an orbit with eccentricity $e = 0.969^{+0.002}_{-0.003}$, at a distance
 558 $a = 3666.195^{+37.781}_{-17.177}$ from its parent stars, with its inclination axis $\omega = 4.144^{+0.547}_{-0.347}$.

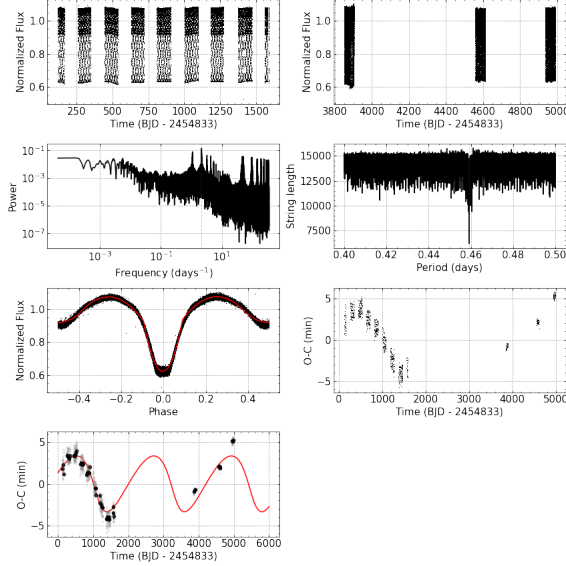


Figure 61. O-C diagram for the binary system KIC 9083523 (TIC 159169838).

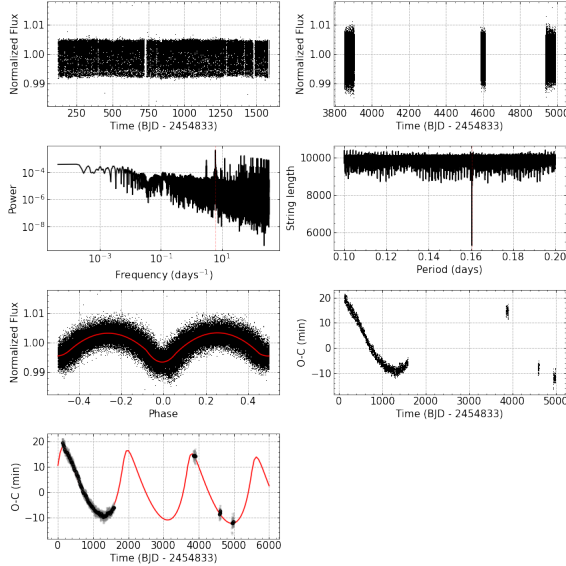


Figure 62. O-C diagram for the binary system KIC 9181877 (TIC 239309691).

A.55. *KIC 9402652 (TIC 159723646) Object*

This object presents a periodic variation in its O-C diagram, Fig. 64, intuiting the presence of a third body around the binary system with a period $P = 1499.321^{+2.076}_{-2.039}$, in an orbit with eccentricity $e = 0.817^{+0.028}_{-0.034}$, at a distance $a = 1473.178^{+38.354}_{-37.486}$ from its parent stars, with its inclination axis $\omega = 263.772^{+1.795}_{-2.034}$.

A.56. *KIC 9451096 (TIC 164784457) Object*

This object presents a periodic variation in its O-C diagram, Fig. 66, intuiting the presence of a third body around the binary system with a period $P =$, in an orbit with eccentricity $e =$, at a distance $a =$ from its parent stars, with its inclination axis $\omega =$.

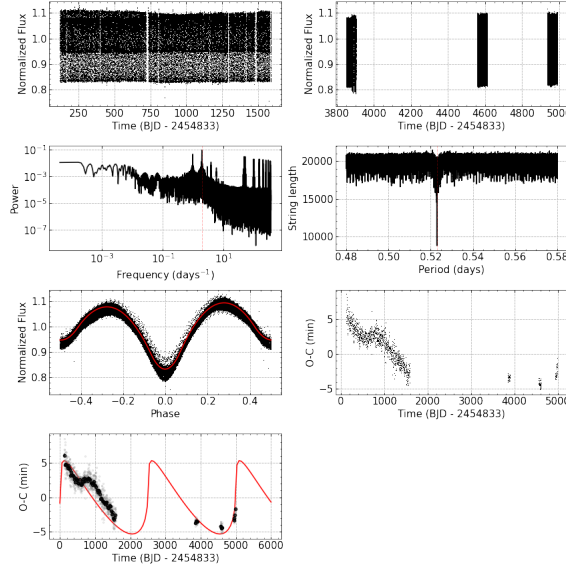


Figure 63. O-C diagram for the binary system KIC 9345838 (TIC 275575030).

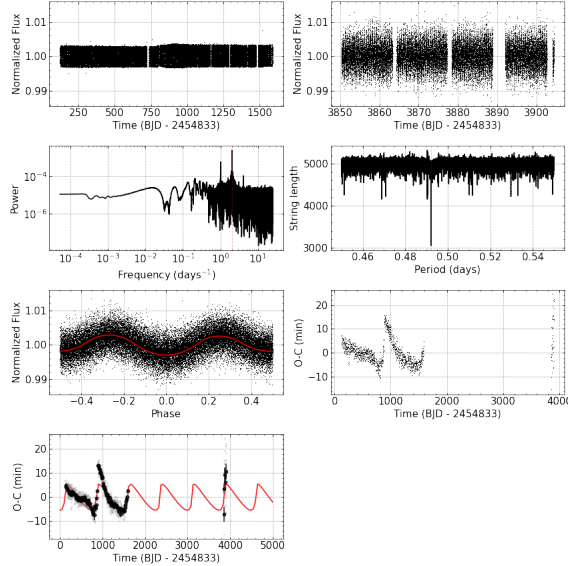


Figure 64. Same analyses of Fig. 11, but for KIC 9365025 (TIC 268711288).

A.57. *KIC 9602595 (TIC 273043307) Object*

567 This object presents a periodic variation in its O-C diagram, Fig. 67, intuiting the presence of a third body around
 568 the binary system with a period $P = 6556.627^{+175.520}_{-624.070}$, in an orbit with eccentricity $e = 0.762^{+0.037}_{-0.028}$, at a distance
 569 $a = 37057.818^{+1690.472}_{-1659.916}$ from its parent stars, with its inclination axis $\omega = 191.337^{+7.883}_{-4.892}$.

A.58. *KIC 9612468 (TIC 239233211) Object*

571 This object presents a periodic variation in its O-C diagram, Fig. 68, intuiting the presence of a third body around
 572 the binary system with a period $P = 7444.129^{+487.713}_{-417.057}$, in an orbit with eccentricity $e = 0.620^{+0.044}_{-0.051}$, at a distance
 573 $a = 1124.834^{+45.727}_{-41.955}$ from its parent stars, with its inclination axis $\omega = 138.663^{+6.605}_{-7.099}$.

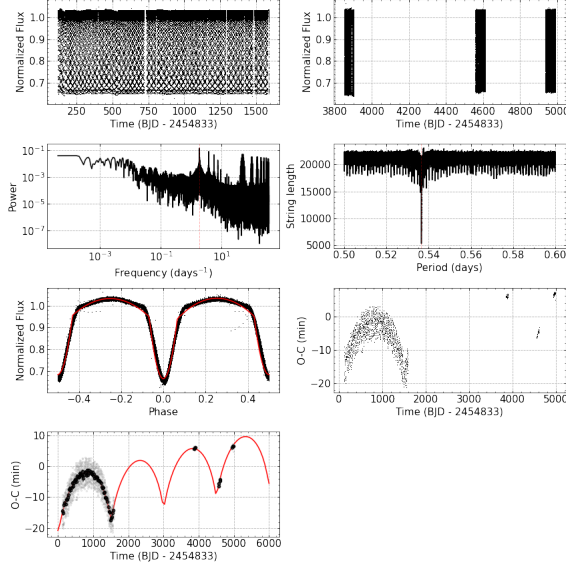


Figure 65. O-C diagram for the binary system KIC 9402652 (TIC 159723646).

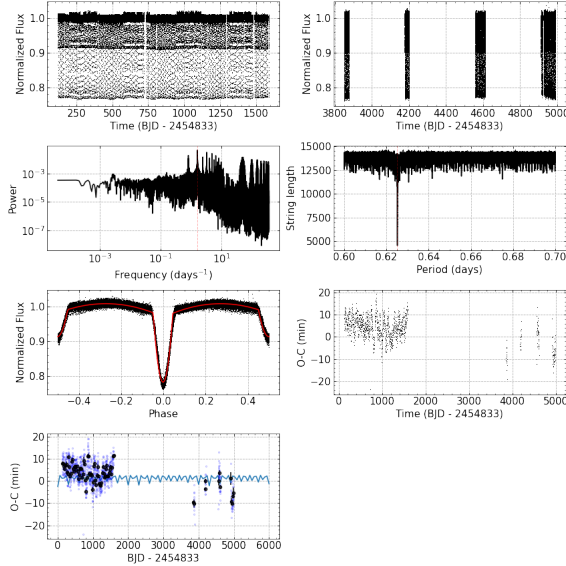


Figure 66. O-C diagram for the binary system KIC 9451096 (TIC 164784457).

A.59. *KIC 9657096 (TIC 271354390) Object*

575 This object presents a periodic variation in its O-C diagram, Fig. 69, intuiting the presence of a third body around
 576 the binary system with a period $P = 1829.705^{+96.740}_{-26.635}$, in an orbit with eccentricity $e = 0.607^{+0.034}_{-0.077}$, at a distance
 578 $a = 1929.070^{+47.691}_{-45.751}$ from its parent stars, with its inclination axis $\omega = 132.949^{+8.377}_{-4.699}$.

A.60. *KIC 9760531 (TIC 158321712) Object*

580 This object presents a periodic variation in its O-C diagram, Fig. 70, intuiting the presence of a third body around
 581 the binary system with a period $P = 2984.870^{+23.366}_{-31.904}$, in an orbit with eccentricity $e = 0.960^{+0.006}_{-0.095}$, at a distance
 582 $a = 886.002^{+45.537}_{-122.871}$ from its parent stars, with its inclination axis $\omega = 15.153^{+18.866}_{-4.047}$.

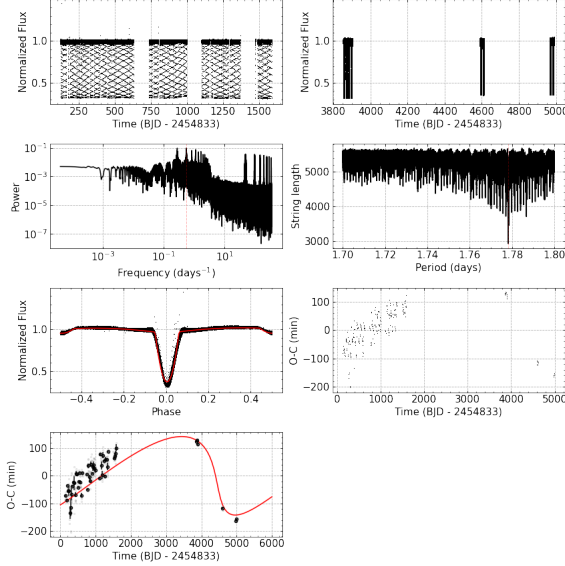


Figure 67. O-C diagram for the binary system KIC 9602595 (TIC 273043307).

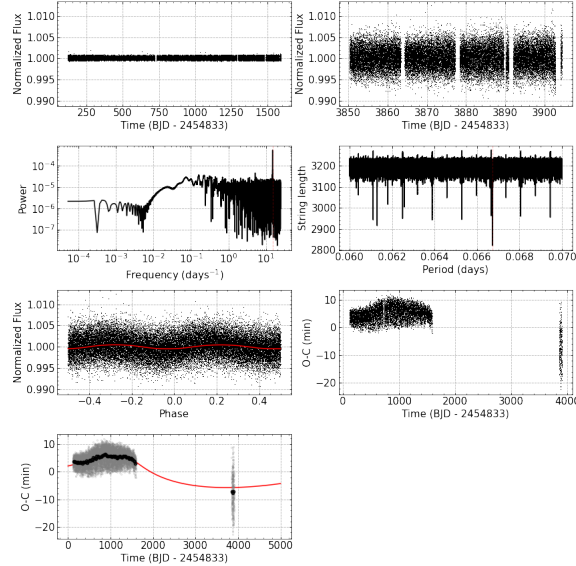


Figure 68. O-C diagram for the binary system KIC 9612468 (TIC 239233211).

583

A.61. *KIC 9832227 (TIC 63205800) Object*

584 This object presents a periodic variation in its O-C diagram, Fig. 71, intuiting the presence of a third body around
 585 the binary system with a period $P = 6091.433^{+142.763}_{-115.053}$, in an orbit with eccentricity $e = 0.507^{+0.028}_{-0.047}$, at a distance
 586 $a = 4066.124^{+32.655}_{-168.895}$ from its parent stars, with its inclination axis $\omega = 313.916^{+1.271}_{-5.992}$.

587

A.62. *KIC 10155563 (TIC 63205800) Object*

588 This object presents a periodic variation in its O-C diagram, Fig. 72, intuiting the presence of a third body around
 589 the binary system with a period $P = 3569.345^{+16.637}_{-16.118}$, in an orbit with eccentricity $e = 0.989^{+0.001}_{-0.002}$, at a distance
 590 $a = 1719.462^{+363.269}_{-295.336}$ from its parent stars, with its inclination axis $\omega = 218.980^{+10.329}_{-6.680}$.

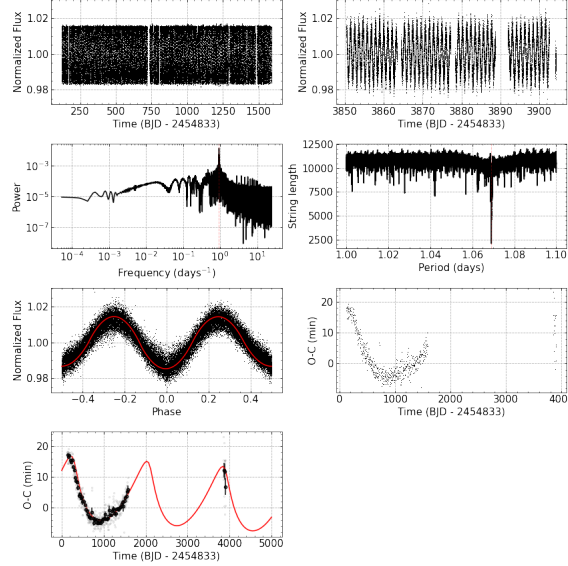


Figure 69. O-C diagram for the binary system KIC 9657096 (TIC 271354390).

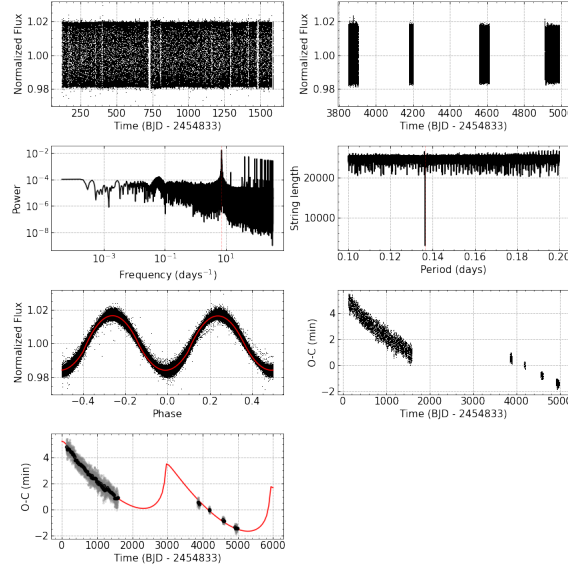


Figure 70. O-C diagram for the binary system KIC 9760531 (TIC 158321712).

591 A.63. *KIC 10226388 (TIC 273872891) Object*

592 This object presents a periodic variation in its O-C diagram, Fig. 73, intuiting the presence of a third body around
 593 the binary system with a period $P = 924.443^{+9.411}_{-1.880}$, in an orbit with eccentricity $e = 0.518^{+0.238}_{-0.031}$, at a distance
 594 $a = 1402.755^{+308.527}_{-174.692}$ from its parent stars, with its inclination axis $\omega = 73.461^{+5.698}_{-11.645}$.

595 A.64. *KIC 10259530 (TIC 164833847) Object*

596 This object presents a periodic variation in its O-C diagram, Fig. 74, intuiting the presence of a third body around
 597 the binary system with a period $P = 4636.848^{+95.939}_{-92.547}$, in an orbit with eccentricity $e = 0.561^{+0.028}_{-0.173}$, at a distance
 598 $a = 381.542^{+18.713}_{-25.245}$ from its parent stars, with its inclination axis $\omega = 100.245^{+11.074}_{-21.152}$.

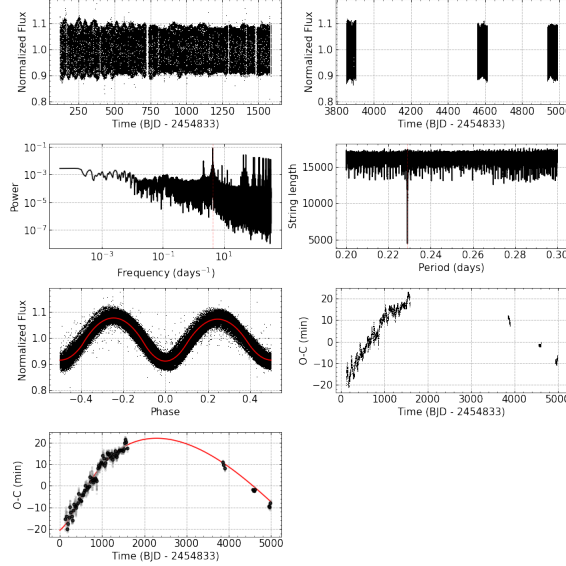


Figure 71. O-C diagram for the binary system KIC 9832227 (TIC 63205800).

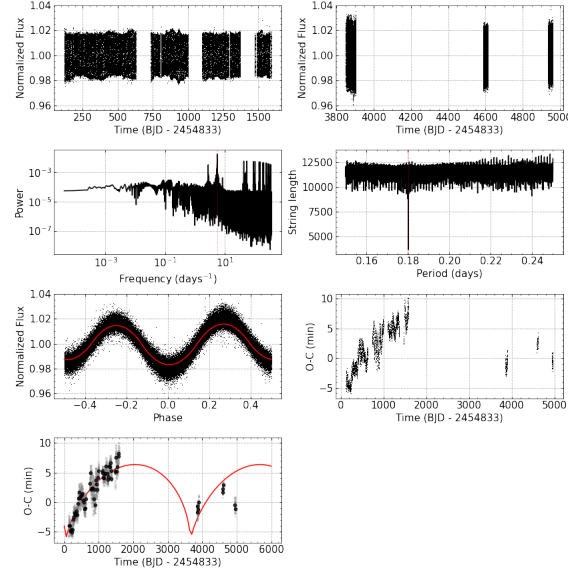


Figure 72. O-C diagram for the binary system KIC 10155563 (TIC 63205800).

A.65. *KIC 10389982 (TIC 164782264) Object*

This object presents a periodic variation in its O-C diagram, Fig. 75, intuiting the presence of a third body around the binary system with a period $P = 2300.442^{+103.102}_{-37.377}$, in an orbit with eccentricity $e = 0.839^{+0.111}_{-0.090}$, at a distance $a = 239.080^{+8.393}_{-14.645}$ from its parent stars, with its inclination axis $\omega = 330.594^{+20.678}_{-14.730}$.

A.66. *KIC 10481912 (TIC 272079818) Object*

This object presents a periodic variation in its O-C diagram, Fig. 76, intuiting the presence of a third body around the binary system with a period $P = 4101.691^{+96.134}_{-510.167}$, in an orbit with eccentricity $e = 0.353^{+0.138}_{-0.120}$, at a distance $a = 543.619^{+43.615}_{-42.953}$ from its parent stars, with its inclination axis $\omega = 56.372^{+36.062}_{-30.249}$.

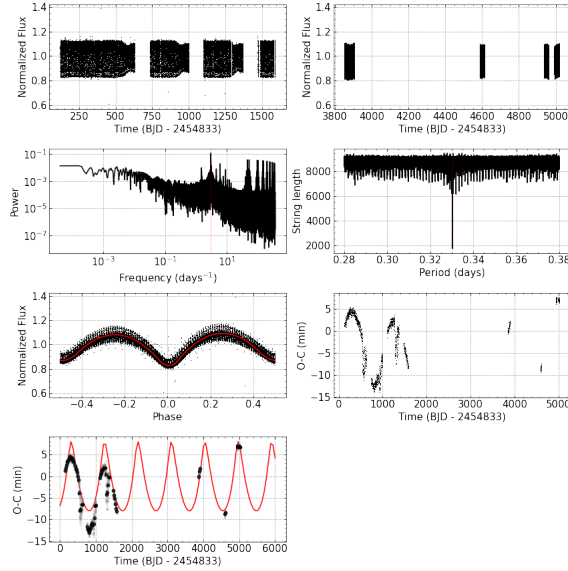


Figure 73. Same analyses of Fig. 11, but for KIC 10226388 (TIC 273872891).

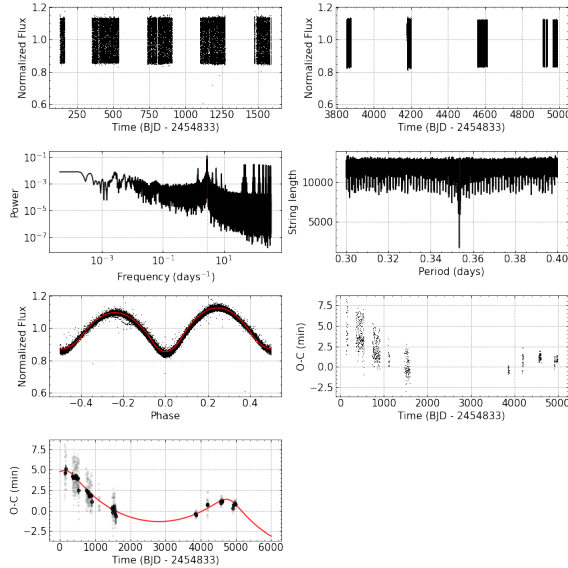


Figure 74. O-C diagram for the binary system KIC 10259530 (TIC 164833847).

A.67. *KIC 10485137 (TIC 272841995) Object*

607 This object presents a periodic variation in its O-C diagram, Fig. 77, intuiting the presence of a third body around
 608 the binary system with a period $P = 5843.721^{+412.625}_{-144.971}$, in an orbit with eccentricity $e = 0.639^{+0.072}_{-0.064}$, at a distance
 609 $a = 1209.034^{+122.158}_{-7.875}$ from its parent stars, with its inclination axis $\omega = 129.134^{+6.999}_{-2.731}$.

A.68. *KIC 10711938 (TIC 48189126) Object*

611 This object presents a periodic variation in its O-C diagram, Fig. 78, intuiting the presence of a third body around
 612 the binary system with a period $P = 6688.888^{+261.034}_{-315.892}$, in an orbit with eccentricity $e = 0.631^{+0.250}_{-0.059}$, at a distance
 613 $a = 1187.255^{+320.546}_{-199.144}$ from its parent stars, with its inclination axis $\omega = 18.743^{+20.175}_{-10.691}$.

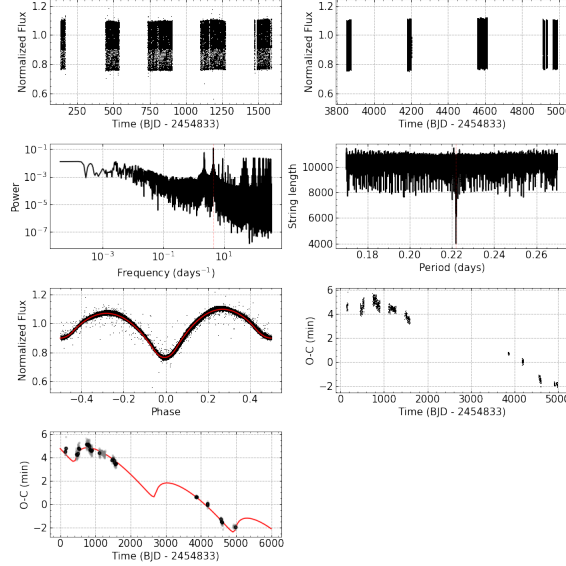


Figure 75. O-C diagram for the binary system KIC 10389982 (TIC 164782264).

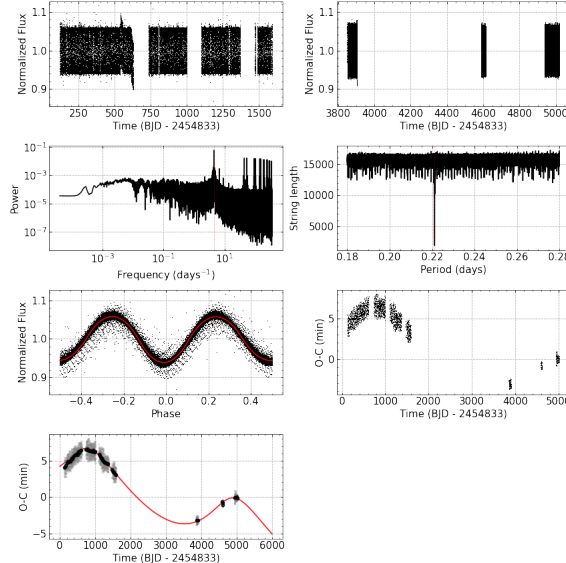


Figure 76. O-C diagram for the binary system KIC 10481912 (TIC 272079818).

615

A.69. *KIC 10724533 (TIC 299156852) Object*

616 This object presents a periodic variation in its O-C diagram, Fig. 79, intuiting the presence of a third body around
 617 the binary system with a period $P = 1936.467^{+52.152}_{-28.855}$, in an orbit with eccentricity $e = 0.426^{+0.035}_{-0.185}$, at a distance
 618 $a = 539.967^{+20.384}_{-38.284}$ from its parent stars, with its inclination axis $\omega = 218.297^{+7.611}_{-178.969}$.

619

A.70. *KIC 10789421 (TIC 299032481) Object*

620 This object presents a periodic variation in its O-C diagram, Fig. 80, intuiting the presence of a third body around
 621 the binary system with a period $P = 455.994^{+10.275}_{-18.197}$, in an orbit with eccentricity $e = 0.517^{+0.281}_{-0.180}$, at a distance
 622 $a = 903.600^{+184.665}_{-97.340}$ from its parent stars, with its inclination axis $\omega = 8.881^{+17.913}_{-7.311}$ and linear parameters fits at
 623 $A = 9.258^{+0.345}_{-0.448}$ and $B = -0.010^{+0.001}_{-0.000}$.

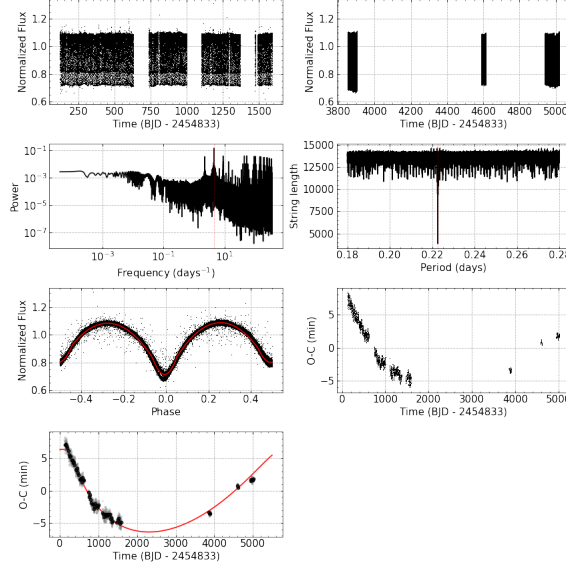


Figure 77. O-C diagram for the binary system KIC 10485137 (TIC 272841995).

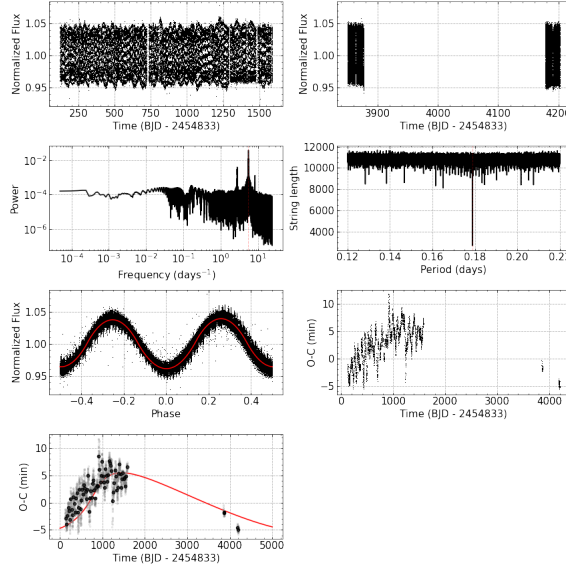


Figure 78. O-C diagram for the binary system KIC 10711938 (TIC 48189126).

624

A.71. *KIC 10818544 (TIC 416528957) Object*

625 This object presents a periodic variation in its O-C diagram, Fig. 81, intuiting the presence of a third body around
 626 the binary system with a period $P = 1892.800^{+120.088}_{-78.434}$, in an orbit with eccentricity $e = 0.967^{+0.011}_{-0.030}$, at a distance
 627 $a = 1050.905^{+160.062}_{-328.243}$ from its parent stars, with its inclination axis $\omega = 356.844^{+2.560}_{-3.514}$.

628

A.72. *KIC 10979669 (TIC 26962050) Object*

629 This object presents a periodic variation in its O-C diagram, Fig. 82, intuiting the presence of a third body around
 630 the binary system with a period $P = 1532.272^{+54.987}_{-20.992}$, in an orbit with eccentricity $e = 0.974^{+0.008}_{-0.013}$, at a distance
 631 $a = 1995.936^{+218.291}_{-463.016}$ from its parent stars, with its inclination axis $\omega = 356.030^{+1.424}_{-2.425}$.

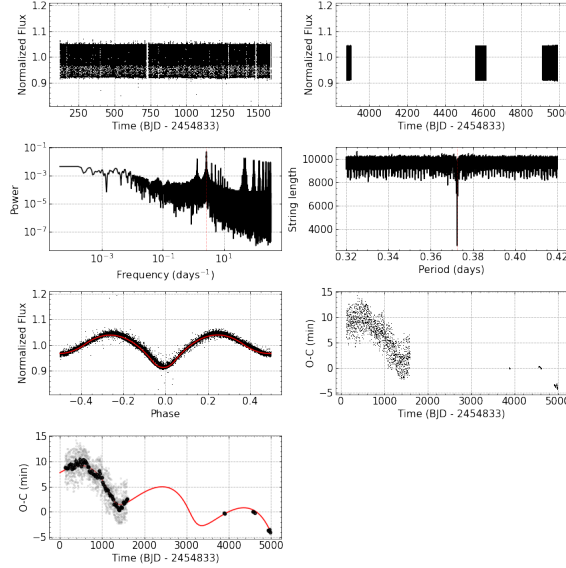


Figure 79. O-C diagram for the binary system KIC 10724533 (TIC 299156852).

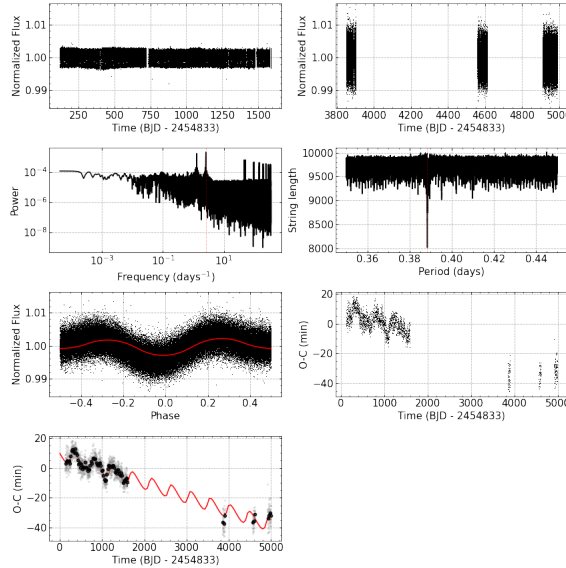


Figure 80. Same analyses of Fig. 11, but for KIC 10789421 (TIC 299032481).

632

A.73. *KIC 10991989 (TIC 264508409) Object*

633 This object presents a periodic variation in its O-C diagram, Fig. 83, intuiting the presence of a third body around
 634 the binary system with a period $P =$, in an orbit with eccentricity $e =$, at a distance $a =$ from its parent stars, with
 635 its inclination axis $\omega =$.

636

A.74. *KIC 11255667 (TIC 27914890) Object*

637 This object presents a periodic variation in its O-C diagram, Fig. 84, intuiting the presence of a third body around
 638 the binary system with a period $P = 4715.408^{+411.622}_{-203.023}$, in an orbit with eccentricity $e = 0.269^{+0.112}_{-0.143}$, at a distance
 639 $a = 674.638^{+58.702}_{-38.804}$ from its parent stars, with its inclination axis $\omega = 331.369^{+16.426}_{-9.484}$.

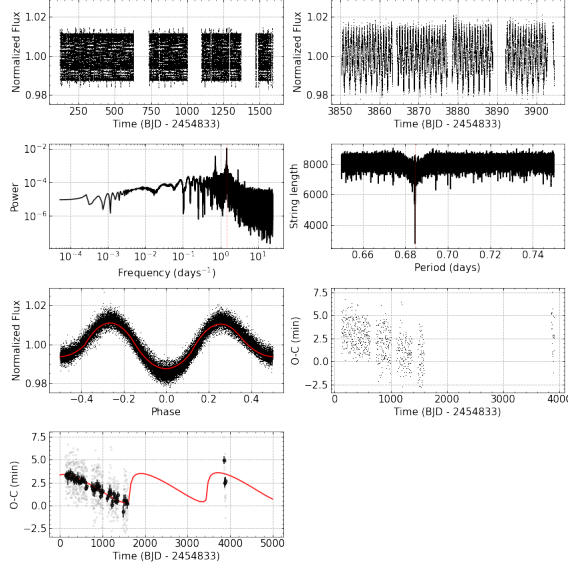


Figure 81. O-C diagram for the binary system KIC 10818544 (TIC 416528957).

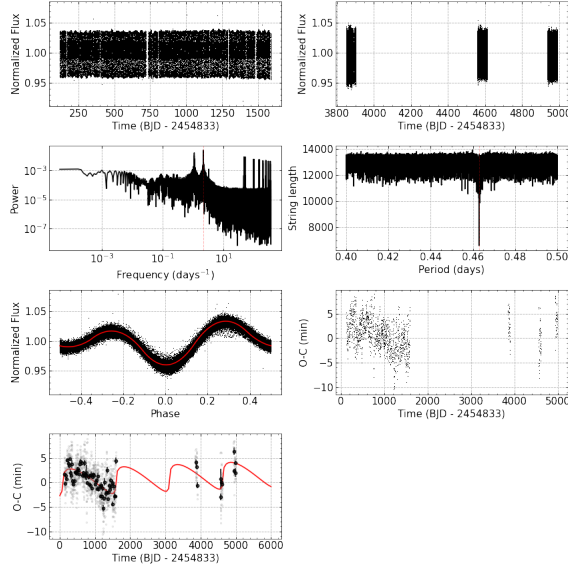


Figure 82. O-C diagram for the binary system KIC 10979669 (TIC 26962050).

A.75. *KIC 11409673 (TIC 27395746) Object*

This object presents a periodic variation in its O-C diagram, Fig. 85, intuiting the presence of a third body around the binary system with a period $P = 5483.304^{+199.637}_{-143.780}$, in an orbit with eccentricity $e = 0.972^{+0.009}_{-0.011}$, at a distance $a = 1566216.412^{+259342.620}_{-189283.693}$ from its parent stars, with its inclination axis $\omega = 182.402^{+1.092}_{-1.396}$.

A.76. *KIC 11572643 (TIC 28306907) Object*

This object presents a periodic variation in its O-C diagram, Fig. 86, intuiting the presence of a third body around the binary system with a period $P = 2290.326^{+48.331}_{-46.637}$, in an orbit with eccentricity $e = 0.503^{+0.314}_{-0.198}$, at a distance $a = 1129.003^{+56.179}_{-112.310}$ from its parent stars, with its inclination axis $\omega = 15.912^{+39.195}_{-14.694}$.

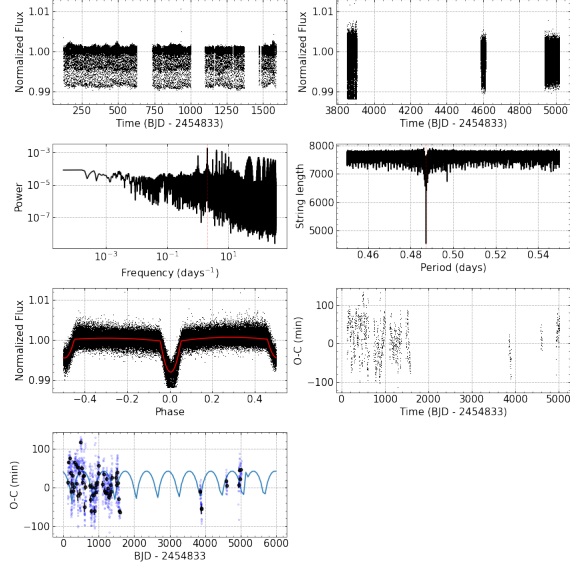


Figure 83. O-C diagram for the binary system KIC 10991989 (TIC 264508409).

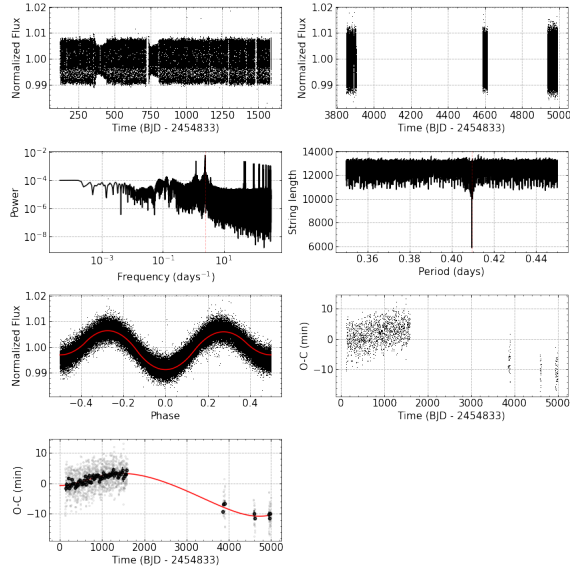


Figure 84. O-C diagram for the binary system KIC 11255667 (TIC 27914890).

648

A.77. *KIC 12216817 (TIC 27639466) Object*

649 This object presents a periodic variation in its O-C diagram, Fig. 87, intuiting the presence of a third body around
 650 the binary system with a period $P = 1508.869^{+27.582}_{-41.085}$, in an orbit with eccentricity $e = 0.619^{+0.071}_{-0.084}$, at a distance
 651 $a = 533.169^{+48.895}_{-41.912}$ from its parent stars, with its inclination axis $\omega = 323.187^{+7.506}_{-10.828}$.

652

A.78. *KIC 12305537 (TIC 406951407) Object*

653 This object presents a periodic variation in its O-C diagram, Fig. 88, intuiting the presence of a third body around
 654 the binary system with a period $P = 2039.912^{+9.942}_{-11.011}$, in an orbit with eccentricity $e = 0.736^{+0.086}_{-0.038}$, at a distance
 655 $a = 2946.364^{+654.431}_{-207.403}$ from its parent stars, with its inclination axis $\omega = 5.025^{+1.976}_{-2.009}$.

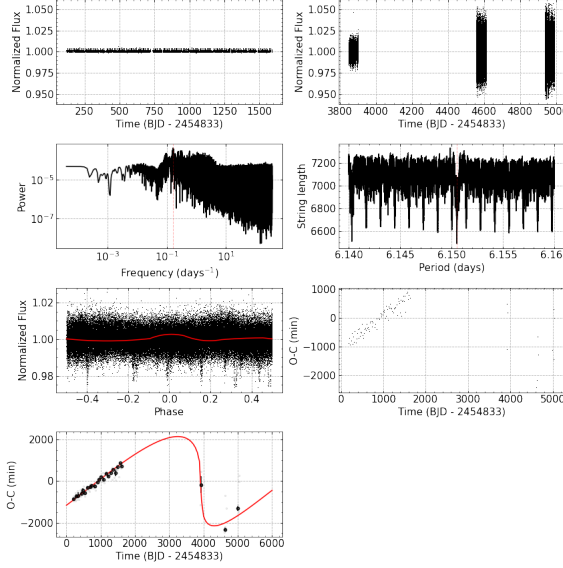


Figure 85. O-C diagram for the binary system KIC 11409673 (TIC 27395746).

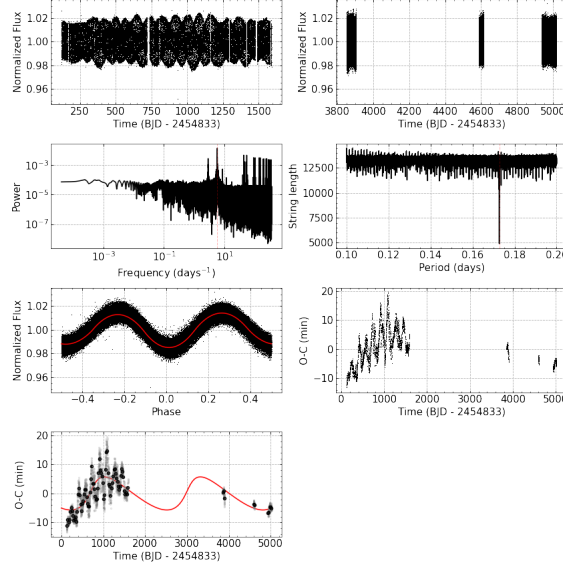


Figure 86. O-C diagram for the binary system KIC 11572643 (TIC 28306907).

B. BINARY SYSTEMS WITH NON-PERIODIC VARIATIONS ON THE O-C DIAGRAM

Through the analysis of the O-C diagram of the binary systems in our sample, we were able to verify and determine variations in certain objects, characterizing periodic variations or not in their orbital periods. Any deviations, whether linear or periodic, in the O-C diagram could indicate changes in the orbital period over time, which could be caused by a variety of factors, such as gravitational interactions with other stars or the presence of a third body around the system.

Thus, we could observe that a percentage of, approximately, 67.5%, that is, 162 systems do not present non-periodic variations in their O-C diagrams. This means that short-term variations in these systems do not represent statistically significant deviations from the assumed orbital period, as determined by the False Alarm Probability (FAP) (VanderPlas 2018). The FAP is a measure of the probability that a given deviation in the O-C diagram is due to chance and not to an actual physical effect.

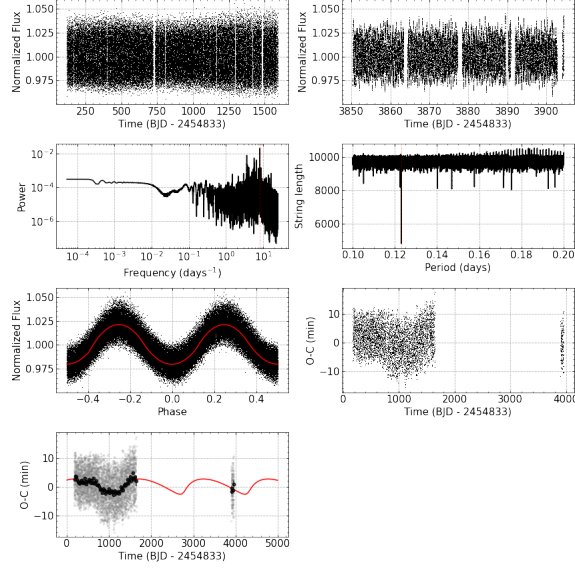


Figure 87. O-C diagram for the binary system KIC 12216817 (TIC 27639466).

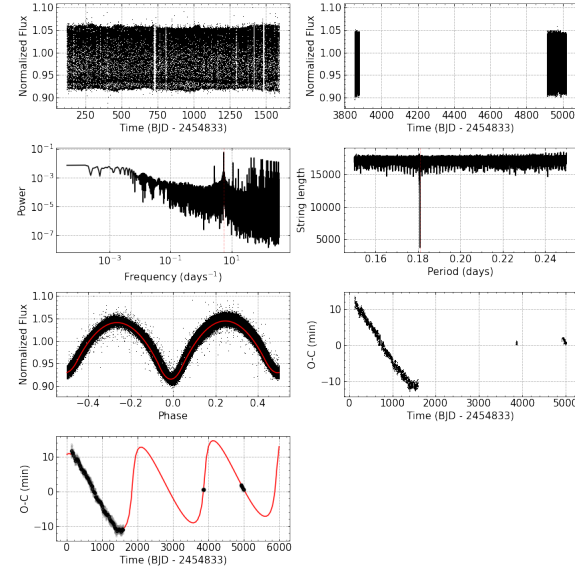


Figure 88. O-C diagram for the binary system KIC 12305537 (TIC 406951407).

667 The absence of significant variations in the O-C diagrams of these 162 systems suggests that their orbital periods
 668 are relatively stable over time. However, it is important to note that this does not necessarily mean that these systems
 669 are completely stable and will not show any long-term changes in their periods. Further observations and analyzes
 670 may be necessary to confirm the stability of these systems over longer timescales.

671 Next, in the Figs. 89-90, all these systems can be visualized with their respective light curves, periodogram,
 672 stringlength, phase light curve and their derived O-C diagram.

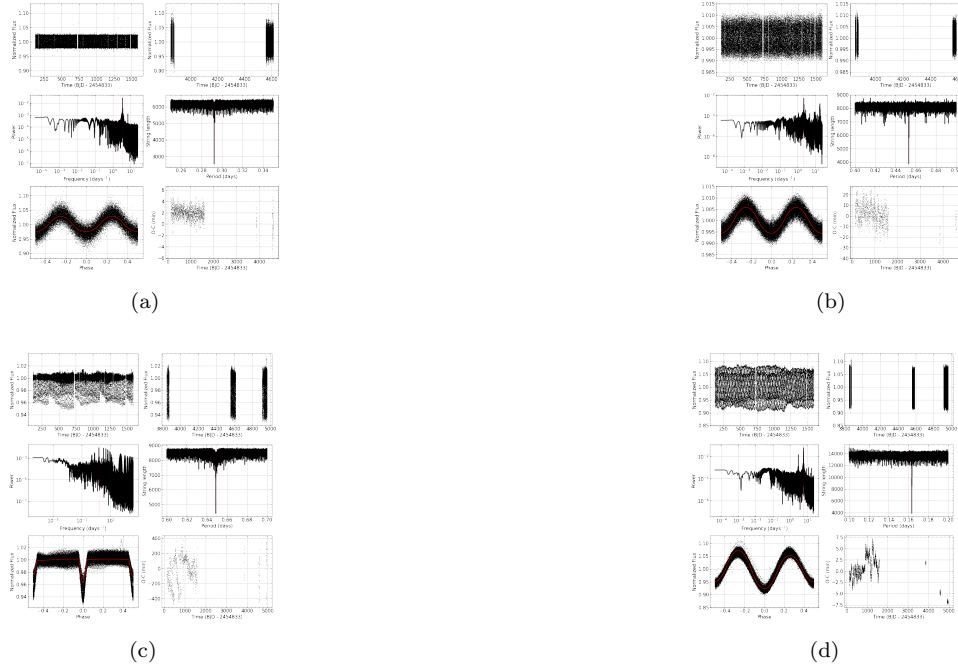


Figure 89.

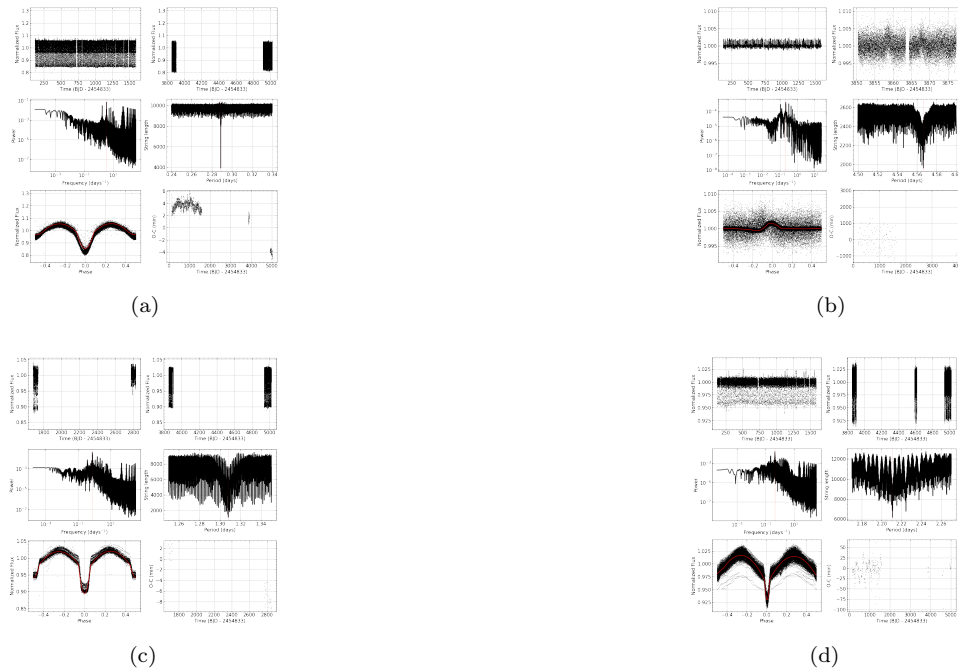


Figure 90.

Table 4. Physical and geometric parameters derived from the binary systems of our sample taken from Conroy et al. (2014). *Our values are indicated in bold

KIC	P_{bin} (days)	P_3 (days)	e_3	P_3^* (days)	e_3^*	a^* (min)	ω^*	A	B
1868650	0.585
2162283	0.906	2307 ⁺⁴⁵ ₋₇₃	0.64 ^{+0.15} _{-0.12}	1321 ⁺³⁶⁷ ₋₂₄₉	307 ⁺²⁷ ₋₄₅	307 ⁺¹⁰ ₋₁₈	307 ⁺¹⁰ ₋₁₈
2450566	1.845	984 ± 473	0.31 ± 0.02	1059 ⁺²³ ₋₂₉	0.655 ^{+0.105} _{-0.066}	1487 ⁺¹⁸² ₋₁₅₁
2557430	1.298
2694741	0.327	1437 ⁺¹⁴ ₋₈	0.087 ^{+0.167} _{-0.065}	3998 ⁺¹¹² ₋₁₉₈	187 ⁺⁸ ₋₄	-18 ⁺² ₋₂	0.007 ^{+0.000} _{-0.000}
2708156	1.891	2254 ⁺⁷² ₋₆₂	0.43 ^{+0.04} _{-0.05}	413 ⁺²⁶ ₋₂₉	69 ⁺²⁵ ₋₂₉	0.711 ^{+0.029} _{-0.125}	0.001 ^{+0.000} _{-0.000}
3221207	0.474	~ 1700	...	664 ⁺⁶ ₋₁₅	0.224 ^{+0.173} _{-0.154}	660 ⁺²⁸ ₋₅₇	261 ⁺²³ ₋₄
3228863	0.731	644 ± 16	0.000 ± 0.003
3431321	1.015
3443519	0.354	8314 ⁺²⁹⁸ ₋₉₀	0.753 ^{+0.051} _{-0.014}	298 ⁺⁷ ₋₅	0.86 ^{+2.64} _{-0.68}
3448245	0.513
3547874	19.698
3558822	1.353
3641446	2.100	229 ± 1	0.000 ± 0.010
3729724	16.375
3735597	1.966
3749404	20.311
3850086	19.105
3936357	0.369	~ 2400	...	2133 ⁺⁶⁸ ₋₄₇	0.120 ^{+0.075} _{-0.061}	470 ⁺¹⁸ ₋₂₅	203 ⁺²⁶ ₋₅₁	-3.3 ^{+0.4} _{-0.2}	0.001 ^{+0.000} _{-0.000}
3953981	0.492	2862 ⁺⁹⁵ ₋₁₂₃	0.223 ^{+0.095} _{-0.069}	221 ⁺²⁰ ₋₁₄	285 ⁺²⁸ ₋₄₂	-0.300 ^{+0.045} _{-0.043}	0.001 ^{+0.000} _{-0.000}
3957477	0.979
4245897	11.258
4247791	4.101
4248941	8.643
4450976	12.048	2546 ⁺¹⁶¹ ₋₂₀₄	0.313 ^{+0.150} _{-0.201}	34367 ⁺²⁴⁵¹ ₋₂₇₀₂	297 ⁺³⁵ ₋₃₄
4451148	0.736	746 ± 52	0.293 ± 0.004	769 ⁺¹¹ ₋₁₉	0.466 ^{+0.087} _{-0.023}	909 ⁺¹⁸⁶ ₋₁₈₃	165 ⁺⁸ ₋₁₄₇	165 ⁺⁸ ₋₁₄₇	165 ⁺⁸ ₋₁₄₇
4647652	1.065	755 ± 44	0.244 ± 0.003	755 ⁺¹⁹ ₋₁₃	0.245 ^{+0.290} _{-0.147}	636 ⁺¹⁴⁷ ₋₁₄₃	239 ⁺⁵⁹ ₋₂₁	239 ⁺⁵⁹ ₋₂₁	239 ⁺⁵⁹ ₋₂₁
4729553	0.961
4743626	1.303
4758368	3.750	~ 1500
4761060	3.363
4850874	1.776
4851217	2.470	2474 ⁺³¹⁸ ₋₁₄₇	0.88 ^{+0.08} _{-0.06}	826 ⁺⁹⁹ ₋₉₉	102 ⁺¹³ ₋₁₂	8.2 ^{+0.7} _{-0.5}	-0.007 ^{+0.001} _{-0.000}
4909422	0.395	6583 ⁺⁹²⁷ ₋₁₄₁₅	0.8 ^{+0.1} _{-0.1}	788 ⁺³⁹ ₋₁₀₀	6.7 ^{+6.8} _{-5.0}	6.1 ^{+0.7} _{-1.3}	-0.002 ^{+0.001} _{-0.000}

Table 4 *continued*

Table 4 (continued)

KIC	P_{bin}	P_3	e_3	P_3^*	e_3^*	a^*	ω^*	A	B
	(days)	(days)		(days)					
4909707	2.302	516 ± 16	0.686 ± 0.006	513.7 ^{+0.6} _{-0.5}	0.66 ^{+0.03} _{-0.05}	2067 ⁺⁷² ₋₆₆	358 ⁺¹ ₋₂₅	-6.86 ^{+0.11} _{-0.11}	0.003 ^{+0.000} _{-0.000}
4945588	1.129	~ 1500	...	1608 ⁺²⁵ ₋₁₄₁	0.87 ^{+0.05} _{-0.05}	1290 ⁺³² ₋₆₇	135 ⁺⁵ ₋₆	9.2 ^{+0.3} _{-0.6}	-0.002 ^{+0.000} _{-0.000}
4949194	41.255
4954113	0.668	21.18 ⁺⁶¹ ₋₃₃	0.72 ^{+0.04} _{-0.03}	429 ⁺²⁵ ₋₄₀	353 ⁺⁵ ₋₁₃	4.7 ^{+0.2} _{-0.2}	-0.002 ^{+0.000} _{-0.000}
4999260	0.378	1827 ⁺¹¹⁴ ₋₁₁₃	0.77 ^{+0.08} _{-0.06}	2900 ⁺²⁷⁵ ₋₂₉₉	26 ⁺¹³ ₋₁₀	2.90 ^{+0.12} _{-0.14}	-0.001 ^{+0.000} _{-0.000}
5022573	0.442
5090937	8.846
5123176	0.708
5197256	6.963
5264818	1.905	300 ± 108	0.42 ± 0.31	282 ⁺³ ₋₄	0.44 ^{+0.21} _{-0.31}	486 ⁺⁵⁹ ₋₁₇₇	342 ⁺¹³ ₋₄₆	3.7 ^{+0.4} _{-0.3}	-0.000 ^{+0.000} _{-0.000}
5296877	0.377	~ 1900	...	4962 ⁺¹¹ ₋₁₆	0.73 ^{+0.01} _{-0.01}	929 ⁺⁵ ₋₆	87.0 ^{+0.7} _{-0.7}
5398002	14.160
5444392	1.520
5458880	3.512
5471619	0.963
5511076	6.514
5513861	1.510	~ 1800	...	2113 ⁺⁶ ₋₆	0.32 ^{+0.02} _{-0.03}	3763 ⁺⁹¹ ₋₈₉	291 ⁺⁵ ₋₆
5598639	1.298
5703230	0.731
5733384	1.547
5771961	26.073
5802834	1.092
5818706	14.957
5821050	1.933
5872696	0.173
5952403	0.906
5975712	1.136	1165 ± 964	0.000 ± 0.013	1694 ⁺² ₋₁	0.218 ^{+0.001} _{-0.001}	171.8 ⁺¹ ₋₂	262.2 ^{+0.4} _{-0.5}	25.815 ^{+0.036} _{-0.014}	-0.012 ^{+0.000} _{-0.000}
5985314	5.354
5988465	3.528
6026204	2.280
6072195	2.800
6105491	13.323
6187893	0.789	~ 7800	...	2029 ⁺⁶ ₋₆	0.969 ^{+0.004} _{-0.002}	15566 ⁺¹¹¹⁷ ₋₁₆₆₀	354 ⁺¹ ₋₁
6205460	3.723	2312 ⁺⁸⁴ ₋₂₉	0.43 ^{+0.06} _{-0.07}	37561 ⁺⁹⁷³ ₋₂₁₅	233 ⁺⁴ ₋₁
63353203	0.509	2450 ⁺¹⁹ ₋₇	0.58 ^{+0.06} _{-0.07}	2535 ⁺¹⁴⁰ ₋₂₆₅	34 ⁺¹⁰ ₋₂
6370558	60.340
6443392	0.777
6447430	1.160

Table 4 continued

Table 4 (*continued*)

KIC	P_{bin}	P_3	e_3	P_3^*	e_3^*	a^*	ω^*	A	B
	(days)	(days)		(days)		(min)			
6462057	0.479	4926 ⁺³⁶⁰ ₋₁₄₇	0.6 ^{+0.1} _{-0.1}	411 ⁺³¹ ₋₄₃	76 ⁺¹⁸ ₋₁₁	1.7 ^{+0.1} _{-0.2}	-0.001 ^{+0.000} _{-0.000}
6669809	0.734
6670812	1.742
6695510	2.173
6699679	0.201
6803335	1.111
6863229	1.995
7023917	0.773
7097571	2.214	4729 ⁺⁴⁴² ₋₁₉₇	0.7 ^{+0.1} _{-0.2}	794 ⁺¹²⁵ ₋₁₇₂	223 ⁺²² ₋₁₇	5.8 ^{+0.8} _{-0.7}	0.001 ^{+0.000} _{-0.000}
7259917	0.385
7284688	0.646
7335517	0.275
7335713	0.574
7350038	13.834
7373255	13.659
7375612	0.160	~2100	...	2123 ⁺¹⁵ ₋₈	0.098 ^{+0.074} _{-0.028}	1222 ⁺⁴⁵ ₋₁₉	303 ⁺³⁹ ₋₁₉
7382250	1.419
7385478	1.655	1389 ± 795	0.245 ± 0.007	1360 ⁺⁷⁶ ₋₁₀₁	0.78 ^{+0.15} _{-0.36}	2892 ⁺²⁸⁸ ₋₆₂₇	60 ⁺²⁴ ₋₂₆	8 ⁺¹ ₋₂	-0.002 ^{+0.000} _{-0.001}
7387296	2.580
7431703	0.573	1820 ⁺⁴³ ₋₁₀₅	0.45 ^{+0.12} _{-0.16}	194 ⁺⁴⁵ ₋₂₃	133 ⁺⁴⁹ ₋₃₈
7440742	0.284	2003 ⁺¹³⁴ ₋₁₀₅	0.983 ^{+0.005} _{-0.006}	3175 ⁺¹³⁰ ₋₂₇₀	11 ⁺⁴ ₋₁	4.0 ^{+0.5} _{-0.4}	0.007 ^{+0.000} _{-0.000}
7457163	0.775	6256 ⁺¹²⁶ ₋₁₃₅	0.53 ^{+0.03} _{-0.04}	2752 ⁺⁴² ₋₆₁	278 ⁺⁸ ₋₄
7512381	0.424	6805 ⁺¹⁹⁴ ₋₁₃₅	0.41 ^{+0.04} _{-0.13}	1298 ⁺¹²⁸ ₋₄₂	341 ⁺⁷ ₋₅
7542091	0.390
7591456	5.836
7630690	0.887
7672068	16.837
7690843	0.786	74.1 ± 0.1	0.233 ± 0.021	2715 ⁺⁶⁰ ₋₇₂	0.8 ^{+0.1} _{-0.2}	2435 ⁺³⁸⁵ ₋₄₉₅	340 ⁺⁸ ₋₁₁	-0.75 ^{+0.13} _{-0.16}	0.000 ^{+0.000} _{-0.000}
7740302	1.154
7765894	3.204	464 ⁺⁴ ₋₅	0.3 ^{+0.1} _{-0.2}	3832 ⁺⁸⁷⁴ ₋₄₀₇	143 ⁺³⁴ ₋₁₇₃
7766185	0.835	1860 ⁺¹⁰⁰ ₋₈₇	0.95 ^{+0.02} _{-0.02}	89 ⁺¹⁰ ₋₁₃	353 ⁺¹⁵ ₋₉	1.44 ^{+0.05} _{-0.04}	-0.001 ^{+0.000} _{-0.000}
7777443	0.885	2328 ⁺²¹⁰ ₋₃₉₈	0.7 ^{+0.1} _{-0.1}	320 ⁺¹⁸ ₋₂₃	61 ⁺³⁶ ₋₂₇	4.5 ^{+0.2} _{-0.5}	-0.001 ^{+0.000} _{-0.000}
7816201	0.575
7830460	3.398
7884842	1.315
7885570	1.729
7887124	32.469
7897952	66.981

Table 4 *continued*

Table 4 (continued)

KIC	P_{bin}	P_3	e_3	P_3^*	e_3^*	a^*	ω^*	A	B
	(days)	(days)		(days)		(min)			
7938870	0.581	21.01^{+32}_{-33}	$0.627^{+0.094}_{-0.025}$	487^{+42}_{-15}	302^{+8}_{-6}	$-7.7^{+0.2}_{-0.2}$	$0.002^{+0.000}_{-0.000}$
7950962	0.827	3085^{+100}_{-117}	$0.08^{+0.05}_{-0.06}$	309^{+18}_{-31}	172^{+4}_{-6}	$2.0^{+0.1}_{-0.2}$	$0.002^{+0.000}_{-0.000}$
7975824	0.404
7976783	1.209
8027591	24.275
8043961	1.559	478 ± 10	0.000 ± 0.005	423^{+2}_{-2}	$0.4^{+0.2}_{-0.1}$	585^{+75}_{-59}	232^{+21}_{-27}
8045121	0.263	939 ± 26	0.000 ± 0.001	891^{+14}_{-18}	$0.35^{+0.09}_{-0.12}$	857^{+130}_{-87}	178^{+32}_{-32}	$0.76^{+0.14}_{-0.07}$	$0.003^{+0.001}_{-0.001}$
8098728	24.500
8189196	2.304	~ 8300	3903^{+25}_{-31}	$0.980^{+0.003}_{-0.004}$	12580^{+931}_{-841}	352^{+1}_{-1}	...
8231231	0.712	~ 1600	1909^{+50}_{-548}	$0.949^{+0.021}_{-0.033}$	2930^{+111}_{-402}	17^{+4}_{-4}	$3.2^{+0.7}_{-0.6}$
8262223	1.613
8285349	0.667	2043^{+16}_{-55}	$0.522^{+0.022}_{-0.218}$	1554^{+37}_{-103}	$0.2^{+0.7}_{-0.2}$...
8382182	1.259
8386865	1.258	293.9 ± 2.8	0.493 ± 0.013	294^{+1}_{-1}	$0.421^{+0.055}_{-0.033}$	544^{+17}_{-19}	141^{+7}_{-6}
8386982	1.258
8397460	1.419	8113^{+510}_{-443}	$0.966^{+0.003}_{-0.003}$	17860^{+1277}_{-1093}	185^{+3}_{-4}	$-3.0^{+0.8}_{-0.6}$
8523194	0.879
8545456	0.315
8579707	0.789	1945^{+204}_{-25}	$0.52^{+0.09}_{-0.04}$	767^{+60}_{-23}	274^{+12}_{-27}	...
8587792	0.368	5493^{+294}_{-278}	$0.38^{+0.05}_{-0.04}$	1207^{+74}_{-72}	320^{+8}_{-7}	$0.2^{+0.2}_{-0.2}$
8590527	0.740
8654097	3.042
8685306	0.808
8696442	12.219
8719324	10.233
8758161	0.998	18453^{+3265}_{-3355}	$0.91^{+0.05}_{-0.07}$	8615^{+1035}_{-1451}	9^{+10}_{-5}	...
8841616	1.680
8848288	5.567
8868650	4.447
8892722	1.794
8894630	1.084	7636^{+351}_{-316}	$0.74^{+0.04}_{-0.03}$	5540^{+503}_{-297}	14^{+4}_{-4}	...
8912468	0.095
9002076	0.481
9007918	1.387
9016693	26.359
9083523	0.918	~ 5200	...	2201^{+36}_{-16}	$0.37^{+0.08}_{-0.09}$	621^{+29}_{-31}	203^{+10}_{-7}
9108579	1.170
9159301	3.045

Table 4 continued

Table 4 (*continued*)

KIC	P_{bin} (days)	P_3 (days)	e_3	P_3^* (days)	e_3^*	a^* (min)	ω^*	A	B
9181877	0.321	~ 2600	...	1830 $^{+20}_{-49}$	0.60 $^{+0.05}_{-0.05}$	2570 $^{+286}_{-144}$	45 $^{+9}_{-10}$	4.7 $^{+0.3}_{-0.5}$	-0.001 $^{+0.000}_{-0.000}$
9220600	0.979
9228778	1.567
9345838	1.046	2497 $^{+5}_{-7}$	0.97 $^{+0.01}_{-0.01}$	3366 $^{+933}_{-754}$	7.0 $^{+0.8}_{-1.2}$
9357275	1.588
9365025	0.984	732 $^{+4}_{-2}$	0.969 $^{+0.002}_{-0.003}$	3666 $^{+38}_{-17}$	4.1 $^{+0.5}_{-0.3}$
9392682	0.893
9394601	0.877
9402652	1.073	1499 $^{+2}_{-2}$	0.82 $^{+0.03}_{-0.03}$	1473 $^{+38}_{-37}$	264 $^{+2}_{-2}$	-12.5 $^{+0.3}_{-0.2}$	0.003 $^{+0.000}_{-0.000}$
9451096	1.250	106.8 \pm 0.1	0.091 \pm 0.033
9470054	1.473
9472174	0.126
9480977	0.871
9512958	3.229
9532855	1.219
9602595	3.556	6557 $^{+176}_{-624}$	0.76 $^{+0.04}_{-0.03}$	37058 $^{+1690}_{-1660}$	191 $^{+8}_{-7}$
9612468	0.133	1264 \pm 233	0.340 \pm 0.001	7444 $^{+188}_{-417}$	0.620 $^{+0.044}_{-0.051}$	1125 $^{+46}_{-42}$	139 $^{+7}_{-7}$
9655187	4.416
9657096	2.138	~ 1400	...	1830 $^{+97}_{-27}$	0.607 $^{+0.034}_{-0.077}$	1929 $^{+48}_{-46}$	133 $^{+8}_{-5}$	6.9 $^{+0.2}_{-0.2}$	-0.001 $^{+0.000}_{-0.000}$
9716456	1.813
9760531	0.273	2985 $^{+23}_{-32}$	0.960 $^{+0.006}_{-0.095}$	886 $^{+46}_{-123}$	15 $^{+19}_{-4}$	3.3 $^{+1.1}_{-0.2}$	-0.001 $^{+0.000}_{-0.000}$
9784371	3.301
9786017	4.498
9788113	2.068
9827122	2.155
9832227	0.458	6091 $^{+143}_{-115}$	0.51 $^{+0.03}_{-0.05}$	4066 $^{+33}_{-169}$	314 $^{+1}_{-6}$
9848190	5.241
9851944	2.164
9898401	0.153
9899216	10.917
9899416	1.333
99006590	1.686
9953894	1.383
9970937	4.875
10000490	1.401
10014536	1.001
10119517	0.737
10149845	4.056

Table 4 *continued*

Table 4 (*continued*)

KIC	P_{bin}	P_3	e_3	P_3^*	e_3^*	a^*	ω^*	A	B
	(days)	(days)		(days)					
1015563	0.360	3569^{+17}_{-16}	$0.989^{+0.001}_{-0.002}$	1719^{+363}_{-295}	219^{+10}_{-7}
10191056	2.427
10206340	4.564
10221886	9.767
10226388	0.661	965 ± 184	0.041 ± 0.007	924^{+9}_{-2}	$0.52^{+0.24}_{-0.03}$	1403^{+309}_{-175}	73^{+6}_{-12}
10235421	0.428
10255530	0.707	4637^{+96}_{-93}	$0.56^{+0.03}_{-0.17}$	382^{+19}_{-25}	100^{+114}_{-21}	$2.82^{+0.13}_{-0.41}$	$-0.001^{+0.000}_{-0.000}$
10274218	1.764
10291683	2.044
10389882	0.444	2300^{+103}_{-37}	$0.84^{+0.11}_{-0.09}$	239^{+8}_{-15}	331^{+21}_{-15}	$5.1^{+0.2}_{-0.2}$	$-0.001^{+0.000}_{-0.000}$
10417986	0.074
10481912	0.442	~ 2700	...	4102^{+96}_{-510}	$0.35^{+0.14}_{-0.12}$	544^{+44}_{-43}	56^{+36}_{-30}	$4.9^{+0.5}_{-0.3}$	$-0.002^{+0.000}_{-0.000}$
10485137	0.445	~ 3100	...	5844^{+413}_{-145}	$0.64^{+0.07}_{-0.06}$	1209^{+122}_{-8}	129^{+7}_{-3}
10556068	2.117
10619109	2.045
10661783	1.231
10684673	0.193
10711938	0.358	~ 2000	...	6689^{+261}_{-316}	$0.63^{+0.25}_{-0.06}$	1187^{+320}_{-199}	19^{+20}_{-18}	$7.412^{+0.985}_{-0.230}$	$-0.002^{+0.000}_{-0.000}$
10724533	0.745	1131 ± 198	0.265 ± 0.003	1936^{+52}_{-29}	$0.43^{+0.04}_{-0.19}$	540^{+20}_{-38}	218^{+18}_{-179}
10735519	0.907
10789421	0.777	456^{+10}_{-18}	$0.52^{+0.28}_{-0.18}$	904^{+185}_{-97}	9^{+18}_{-7}	$9.26^{+0.35}_{-0.45}$	$-0.010^{+0.001}_{-0.000}$
10815379	0.891
10818544	1.369	1893^{+120}_{-78}	$0.97^{+0.01}_{-0.03}$	1051^{+160}_{-328}	357^{+3}_{-4}	$1.81^{+0.15}_{-0.09}$	$0.000^{+0.000}_{-0.000}$
10858720	0.952
10979669	0.926	1532^{+55}_{-21}	$0.974^{+0.008}_{-0.013}$	1996^{+218}_{-463}	3560^{+1}_{-2}	$-0.022^{+0.008}_{-0.002}$	$0.000^{+0.000}_{-0.000}$
10991769	3.281
10991989	0.974	555 ± 64	0.000 ± 0.018
11071278	55.886
11122789	3.238
11135978	0.292
11186361	0.533
11244501	0.297
11255667	0.819	4715^{+412}_{-203}	$0.27^{+0.11}_{-0.14}$	675^{+59}_{-39}	331^{+16}_{-9}	$2.9^{+0.3}_{-0.9}$	$-0.002^{+0.000}_{-0.000}$
11295347	0.888
11403032	7.632	5483^{+200}_{-144}	$0.97^{+0.01}_{-0.01}$	$15662^{+16}_{-189284}$	182^{+1}_{-1}
11409673	12.301
11447953	1.499
11453915	24.214

Table 4 *continued*

Table 4 (continued)

KIC	P_{bin} (days)	P_3 (days)	e_3	P_3^* (days)	e_3^*	a^* (min)	ω^*	A	B
11560447	0.528
11572643	0.345	2290₋₄₇⁺⁴⁸	0.5_{-0.2}^{+0.3}	1129₋₁₁₂⁺⁵⁶	16₋₁₅⁺³⁹
11616594	14.588
11649962	10.564
11769801	29.690
11859811	22.305
11920266	0.467
11923629	17.961
11973705	6.772
12066630	1.098
12157987	0.578	2659₋₃₉⁺⁴⁴	0.92_{-0.12}^{+0.05}	510₋₂₈⁺¹⁷	294₋₁₀⁺⁷	1.92_{-0.04}^{+0.13}	-0.001_{-0.000}^{+0.000}
12216817	0.246	1509₋₄₁⁺²⁸	0.62_{-0.08}^{+0.07}	533₋₄₂⁺⁴⁹	323₋₁₁⁺⁸
12255108	9.134
12257908	2.616
12268220	4.422	2040₋₁₁⁺¹⁰	0.74_{-0.04}^{+0.09}	2946₋₂₀₇⁺⁶⁵⁴	5₋₂⁺²	-0.76_{-0.03}^{+0.02}	0.001_{-0.000}^{+0.000}
12305537	0.362						

REFERENCES

- 674 Almeida, L., Sana, H., de Mink, S., et al. 2015, The
 675 Astrophysical Journal, 812, 102
- 676 Almeida, L., Sana, H., Taylor, W., et al. 2017, Astronomy
 677 & Astrophysics, 598, A84
- 678 Almeida, L. A., de Almeida, L., Damineli, A., et al. 2019,
 679 AJ, 157, 150, doi: [10.3847/1538-3881/ab0963](https://doi.org/10.3847/1538-3881/ab0963)
- 680 Applegate, J. H., & Patterson, J. 1987, The Astrophysical
 681 Journal, 322, L99
- 682 Astudillo-Defru, N., Cloutier, R., Wang, S. X., et al. 2020,
 683 Astronomy & Astrophysics.
<https://api.semanticscholar.org/CorpusID:210920549>
- 685 Batalha, N. M., Borucki, W. J., Bryson, S. T., et al. 2011,
 686 The Astrophysical Journal, 729.
<https://api.semanticscholar.org/CorpusID:55059000>
- 688 Borucki, W. J. 2016, Reports on Progress in Physics, 79.
<https://api.semanticscholar.org/CorpusID:31109219>
- 690 Borucki, W. J., Koch, D., Basri, G., et al. 2010, Science,
 691 327, 977
- 692 Cehula, J., & Pejcha, O. 2023, MNRAS, 524, 471,
 693 doi: [10.1093/mnras/stad1862](https://doi.org/10.1093/mnras/stad1862)
- 694 Clausen, J., Torres, G., Bruntt, H., et al. 2008, Astronomy
 695 & Astrophysics, 487, 1095
- 696 Conroy, K. E., Prša, A., Stassun, K. G., et al. 2014, The
 697 Astronomical Journal, 147, 45
- 698 Correia, A. C., Boué, G., & Laskar, J. 2016, Celestial
 699 Mechanics and Dynamical Astronomy, 126, 189
- 700 Czesla, S., Schröter, S., Schneider, C. P., et al. 2019, PyA:
 701 Python astronomy-related packages.
<http://ascl.net/1906.010>
- 703 Duchêne, G., & Kraus, A. 2013, ARA&A, 51, 269,
 704 doi: [10.1146/annurev-astro-081710-102602](https://doi.org/10.1146/annurev-astro-081710-102602)
- 705 Dworetsky, M. 1983, Monthly Notices of the Royal
 706 Astronomical Society, 203, 917
- 707 Foreman-Mackey, D., Hogg, D. W., Lang, D., & Goodman,
 708 J. 2013, Publications of the Astronomical Society of the
 709 Pacific, 125, 306
- 710 Gandolfi, D., Barragán, O., Livingston, J. W., et al. 2018,
 711 Astronomy & Astrophysics.
- 712 <https://api.semanticscholar.org/CorpusID:119226668>
- 713 Gimenez, A., & Garcia-Pelayo, J. M. 1983, Astrophysics
 714 and Space Science, 92, 203
- 715 Grundahl, F., Clausen, J., Hardis, S., & Frandsen, S. 2008,
 716 Astronomy & Astrophysics, 492, 171
- 717 Hulse, R. A., & Taylor, J. H. 1975, The Astrophysical
 718 Journal, 195, L51
- 719 Irwin, J. B. 1952, The Astrophysical Journal, 116, 211
- 720 Lightkurve Collaboration, Cardoso, J. V. d. M., Hedges, C.,
 721 et al. 2018, Lightkurve: Kepler and TESS time series
 722 analysis in Python, Astrophysics Source Code Library.
<http://ascl.net/1812.013>
- 724 Lomb, N. R. 1976, Astrophysics and space science, 39, 447
- 725 Martin, D. V., & Triaud, A. H. 2015, Monthly Notices of
 726 the Royal Astronomical Society: Letters, 455, L46
- 727 Pietrzyński, G., Gieren, W., Graczyk, D., et al. 2012,
 728 Proceedings of the International Astronomical Union, 8,
 729 169
- 730 Prša, A., Guinan, E., Devinney, E., et al. 2008, The
 731 Astrophysical Journal, 687, 542
- 732 Ricker, G. R., Winn, J. N., Vanderspek, R., et al. 2014,
 733 Journal of Astronomical Telescopes, Instruments, and
 734 Systems, 1, 014003
- 735 Sana, H. 2016, Proceedings of the International
 736 Astronomical Union, 12, 110
- 737 Sana, H., & Evans, C. J. 2010, Proceedings of the
 738 International Astronomical Union, 6, 474
- 739 Sana, H., De Mink, S., de Koter, A., et al. 2012, Science,
 740 337, 444
- 741 Scargle, J. D. 1982, The Astrophysical Journal, 263, 835
- 742 Tokovinin, A. 1997, Astronomy Letters, 23, 727
- 743 Tokovinin, A., Thomas, S., Sterzik, M., & Udry, S. 2006,
 744 Astronomy & Astrophysics, 450, 681
- 745 Tout, C. A., & Hall, D. S. 1991, Monthly Notices of the
 746 Royal Astronomical Society, 253, 9
- 747 VanderPlas, J. T. 2018, The Astrophysical Journal
 748 Supplement Series, 236, 16